

CALT-TH/2026-002
January 2026

Classical equipartition dynamics between axions and non-Abelian gauge fields

Kim V. Berghaus^a, Adrien Florio^b, M. Laine^c, Franz R. Sattler^b

^a*Walter Burke Institute for Theoretical Physics,
California Institute of Technology, CA 91125, USA*

^b*Fakultät für Physik, Universität Bielefeld, D-33615 Bielefeld, Germany*

^c*AEC, Institute for Theoretical Physics, University of Bern,
Sidlerstrasse 5, CH-3012 Bern, Switzerland*

Abstract

Motivated by axion-like inflation and its warm embedding within the Standard Model, we study the early stages of the energy transfer between an axion condensate and an SU(2) gauge ensemble, by employing non-linear classical real-time lattice simulations. The discretized equations of motion are worked out, elaborating on Gauss constraints. A numerical solution is implemented on the CosmoLattice platform. Adopting a quadratic potential, and omitting universe expansion for the moment, we establish initial exponential growth of the low-momentum gauge modes; damping of axion oscillations after some delay; and subsequent energy equipartition between axion and gauge ensembles. A clear difference between the SU(2) and U(1) dynamics is observed, likely associated with non-Abelian self-interactions. We elaborate on what this implies for the possible thermalization of the SU(2) ensemble.

Contents

1	Introduction	1
2	Summary of setup	3
3	Perturbative expectations	6
4	Numerical implementation	8
4.1	Spatial discretization	8
4.2	Time discretization and finite-volume effects	8
4.3	Initial conditions and power spectra	9
5	Early stages of equilibration	9
5.1	Exponential growth of gauge-field energy density	10
5.2	Damping of axion oscillations	11
5.3	Power spectra and energy equipartition	13
6	Conclusions and outlook	16
A	Equations of motion in continuum	19
B	Equations of motion on a spatial lattice	23
B.1	Notation and canonical coordinates	23
B.2	Gauss constraint and Hamiltonian	25
B.3	Evolution equations	26
B.4	Energy conservation	29
B.5	Time dependence of the Gauss constraint	29
B.6	Initial conditions and power spectra	31

1. Introduction

Steady improvements in cosmological data [1–3] are making inflationary model building ever more interesting. From the theoretical perspective, one particularly nice class of models falls under the name of natural inflation [4], where the desired flatness of the inflationary potential is guaranteed by a shift symmetry. The inflaton is then typically a pseudoscalar field, reminiscent of the QCD axion, originally proposed to exist for other reasons [5–7]. Though explicit constructions are not quite easy to formulate (cf., e.g., ref. [8] for the past status), this general class of models has become rather popular in recent years.

An axion-like field couples to the topological charge density, $F\tilde{F}$, of all available gauge fields. Much work has been devoted to the coupling to Abelian fields, as the associated tachyonic instability may lead to spectacular signatures [9, 10]. In the meanwhile, these studies have reached an advanced level, with numerical simulations offering a tool for fully capturing the non-linear dynamics (cf., e.g., refs. [11–14] and references therein).

However, the dynamics experienced by non-Abelian fields could differ from the Abelian case. Non-Abelian gauge covariance induces momentum-dependent cubic self-interactions, which drive rapid equilibration [15]. Though a large Hubble rate poses a challenge for this, it is still interesting to ask what happened if equilibration were reached (cf., e.g., refs. [16–19]). It turns out that the so-called sphaleron processes of the non-Abelian plasma generate a thermal friction for the slowly evolving axion condensate [20, 21]. Estimates of the sphaleron rate in a weakly coupled SU(3) plasma have been obtained with classical real-time lattice simulations [22, 23]. Making use of them, a scenario of warm inflation can be implemented [24], with the regular objections [25] avoided by the approximate shift symmetry. In particular, given an improved understanding of warm-inflation curvature power spectra [26–30], it can be shown that successful warm inflation can be achieved with the QCD axion coupling [31] (see also refs. [30, 32]), utilizing a quartic UV potential that would be excluded without the help of the thermal friction. This class of models makes characteristic predictions about other standard observables, like non-Gaussianities [26, 33, 34], gravitational waves [35–39], or maximal post-inflationary temperatures [40].

We may wonder to what extent all of this depends on whether the system actually equilibrates. Like in the Abelian case with the tachyonic instability, some energy transfer certainly takes place between the axion condensate and long-wavelength gauge fields. In a non-Abelian situation, self-interactions due to cubic and quartic gauge vertices should efficiently redistribute the energy insertions. As the instability band lies at small momenta, the redistributed energy will also initially be in the long-wavelength modes. It is precisely the long-wavelength gauge fields that are responsible for the sphaleron processes, so we might expect that an analogue thereof could also exist in a non-equilibrium setting.

The purpose of our study is to simulate the non-equilibrium dynamics numerically. To show how the relevant observables can be extracted, we first do this in Minkowskian spacetime, where Hubble damping does not complicate the interpretation. We span the regime from underdamped to overdamped oscillations, with the former giving some insight into early matter domination dynamics, and the latter resembling more closely what happens during inflation. In particular, from the overdamped regime we can draw first parallels to warm inflation, which we hope to consolidate in a future study that includes Hubble expansion.

Given that we are not aware of previous numerical simulations of the very same framework, we also invest some effort in spelling out its conceptual and technical foundations. That said, the non-Abelian setup has been studied perturbatively in the inflationary context (cf., e.g.,

refs. [41, 42]), and there are also numerical investigations which did include a non-Abelian $F\bar{F}$ -operator (cf., e.g., ref. [43] and references therein), though in the latter case as a small correction to dynamics that was dominated by renormalizable gauge interactions.

Our presentation is organized as follows. We start by summarizing our setup in continuum notation (cf. sec. 2). Subsequently, some key features of the early-time solution are worked out semi-analytically (cf. sec. 3). We then present the implementation (cf. sec. 4) and main findings (cf. sec. 5) from our non-linear simulations. After drawing conclusions and offering an outlook (cf. appendix 6), we turn to a detailed specification of the equations of motion and the associated conservation laws, first in continuum (cf. appendix A), and then in the presence of a spatial lattice discretization (cf. appendix B).

2. Summary of setup

We consider a system consisting of a pseudoscalar field, $\varphi \in \mathbb{R}$, and non-Abelian gauge fields. The φ is assumed neutral with respect to the gauge group. The Lagrangian density reads

$$\mathcal{L} = \frac{1}{2} \partial^\mu \varphi \partial_\mu \varphi - V(\varphi) - \frac{1}{4} F_{\mu\nu}^a F^{a\mu\nu} - \frac{\varphi \chi}{f_a}, \quad (2.1)$$

where χ is the topological charge density,

$$\chi \equiv \frac{\epsilon^{\mu\nu\rho\sigma} g^2 F_{\mu\nu}^a F_{\rho\sigma}^a}{64\pi^2}. \quad (2.2)$$

Here, we have assumed the metric signature $(+---)$; $F_{\mu\nu}^a$ is the Yang-Mills field strength, with $a = 1, \dots, N_c^2 - 1$ labelling the generators; $\epsilon^{0123} = 1$; and $g^2 = 4\pi\alpha$ is the gauge coupling. To reduce the numerical cost, we focus on $N_c = 2$ in the present study, even though for warm inflation with the QCD axion, $N_c = 3$ would be the relevant case. In order to simplify the equations, we parametrize the coupling between φ and the gauge fields via

$$\kappa \equiv \frac{8g^2}{64\pi^2 f_a} \equiv \frac{\alpha}{2\pi f_a}, \quad (2.3)$$

such that the axion–gauge interaction reads

$$\mathcal{L} \supset -\frac{\kappa\varphi}{8} \epsilon^{\mu\nu\rho\sigma} F_{\mu\nu}^a F_{\rho\sigma}^a = -\frac{\kappa\varphi}{2} \epsilon^{0ijk} F_{0i}^a F_{jk}^a \stackrel{(A.2)}{\equiv} -\kappa\varphi F_{0i}^a B_i^a, \quad (2.4)$$

where $B_i^a \equiv \frac{1}{2} \epsilon_{ijk} F_{jk}^a$ denotes a non-Abelian magnetic field.

The equations of motion following from the Lagrangian in eq. (2.1) are derived in appendix A. Doing a partial fixing to the gauge $A_0^a = 0$, and taking the spatial gauge potentials, A_i^a , as the canonical variables, the would-be Euler-Lagrange equation for A_0^a yields the *Gauss constraint* that needs to be satisfied at the initial time,

$$\mathcal{D} \cdot \mathbf{E} \stackrel{(A.5)}{=} \kappa (\nabla \varphi) \cdot \mathbf{B}, \quad (2.5)$$

where \mathbf{E} and \mathbf{B} are vectors both in gauge algebra and physical space, and \mathcal{D} is the covariant derivative in the adjoint representation. The fact that \mathbf{E} and \mathbf{B} are defined in terms of gauge potentials, leads to two *Jacobi identities*,

$$\mathcal{D} \cdot \mathbf{B} \stackrel{(A.6)}{=} 0, \quad \dot{\mathbf{B}} \stackrel{(A.13)}{=} \mathcal{D} \times \mathbf{E}. \quad (2.6)$$

Finally, the Euler-Lagrange equations for φ and A_i^a , together with the definition of E_i^a from eq. (A.2), yield the evolution equations for the dynamical variables,

$$\ddot{\varphi} \stackrel{(A.14)}{=} \nabla^2 \varphi - V'(\varphi) - \kappa \mathbf{E} \cdot \mathbf{B}, \quad (2.7)$$

$$\dot{\mathbf{A}} \stackrel{(A.15)}{=} \mathbf{E}, \quad (2.8)$$

$$\dot{\mathbf{E}} \stackrel{(A.16)}{=} -\mathcal{D} \times \mathbf{B} + \kappa(\dot{\varphi} \mathbf{B} - \nabla \varphi \times \mathbf{E}). \quad (2.9)$$

To solve the evolution equations, we need to set initial conditions at time $t = 0$. Motivated by the theory of cosmological inflation, we insert there a spatially constant condensate, $\varphi(t, \mathbf{x}) \rightarrow \bar{\varphi}(t)$, which carries almost all of the original energy density. We choose a quadratic potential for the axion,

$$V(\varphi) \equiv \frac{m^2 \varphi^2}{2}. \quad (2.10)$$

For $\kappa = 0$, eq. (2.7) then implies the presence of oscillations. It is convenient to start the evolution at a moment when the condensate crosses zero, so we impose

$$\bar{\varphi}(0) = 0, \quad \dot{\bar{\varphi}}(0) \neq 0. \quad (2.11)$$

We can then assume that the condensate is time-asymmetric, $\bar{\varphi}(-t) = -\bar{\varphi}(t)$.

Apart from the condensate, we also insert some noise at non-zero momenta at $t = 0$ (otherwise the gauge fields stay at zero). It is conventional to mimick quantum fluctuations with such noise [44]. We thus write down an analogue of a mode expansion,

$$\varphi(0, \mathbf{x}) = \int_{\mathbf{k}} \left[c_{\mathbf{k}} \varphi_k(0) e^{i\mathbf{k} \cdot \mathbf{x}} + c_{\mathbf{k}}^* \varphi_k^*(0) e^{-i\mathbf{k} \cdot \mathbf{x}} \right], \quad \int_{\mathbf{k}} \equiv \int \frac{d^3 \mathbf{k}}{(2\pi)^3}, \quad (2.12)$$

$$\dot{\varphi}(0, \mathbf{x}) = \int_{\mathbf{k}} (i\omega_k) \left[-c_{\mathbf{k}} \varphi_k(0) e^{i\mathbf{k} \cdot \mathbf{x}} + c_{\mathbf{k}}^* \varphi_k^*(0) e^{-i\mathbf{k} \cdot \mathbf{x}} \right], \quad (2.13)$$

where $c_{\mathbf{k}}$ are complex random numbers, with $\langle c_{\mathbf{k}} \rangle \equiv 0$, and $\varphi_k(t)$ is a forward-propagating mode function, $\varphi_k(t) \equiv e^{-i\omega_k t} / \sqrt{2\omega_k}$ (cf. eq. (A.20)).

When modelling quantum fluctuations through classical fields, there is an issue of a factor 1/2 (cf. the discussion below eq. (A.22)). There are various possibilities for overcoming this,

such as restricting to $1/2$ of the full momentum space [44]; dividing the quantum mode functions by $\sqrt{2}$ [45]; or simply inserting an extra factor in the noise variance,

$$\langle c_{\mathbf{k}} c_{\mathbf{q}} \rangle = 0, \quad \langle c_{\mathbf{k}} c_{\mathbf{q}}^* \rangle = f_k (2\pi)^3 \delta^{(3)}(\mathbf{k} - \mathbf{q}), \quad f_k \equiv \frac{\theta(\Lambda - k)}{2}. \quad (2.14)$$

We have used f_k to also impose an upper cutoff, Λ , on the momentum range, because classical field theory suffers from a Rayleigh-Jeans divergence, and does not describe correctly large momenta (physically, $k \geq T$). In the present study, as we focus on classical field dynamics, we have further drastically reduced the amplitude of the noise, setting

$$f_k \rightarrow 10^{-10} \theta(\Lambda - k). \quad (2.15)$$

For the gauge sector, we insert no background value in the initial state (however, nothing prohibits one from being generated dynamically under the right conditions, as suggested in refs. [46, 47]). We insert noise in the electric field, in analogy with eq. (2.12); the details are given in eqs. (A.24) [in continuum notation] and (B.63) [in lattice notation]. The initial magnetic fields, B_i^a , are set to zero, so as to satisfy the Gauss constraint from eq. (2.5). Non-zero B_i^a arise rapidly from the dynamics, as implied by eq. (2.8). We remark that our qualitative results are stable in the class of initial conditions that satisfy the Gauss constraint.

Among the most important observables that we measure are the *power spectra* associated with different fields. Focussing on the example of φ , we recall that in a translationally invariant system, statistical averages only depend on relative separations, $\langle \varphi(t, \mathbf{x}) \varphi(t, \mathbf{y}) \rangle = \mathcal{F}(\mathbf{x} - \mathbf{y})$. For the corresponding Fourier transforms, $\varphi(t, \mathbf{k}) \equiv \int_{\mathbf{x}} e^{-i\mathbf{k}\cdot\mathbf{x}} \varphi(t, \mathbf{x})$, where $\int_{\mathbf{x}} \equiv \int d^3x$, this implies that

$$\langle \varphi(t, \mathbf{k}) \varphi^*(t, \mathbf{q}) \rangle = (2\pi)^3 \delta^{(3)}(\mathbf{k} - \mathbf{q}) G_{\varphi}(t, \mathbf{k}), \quad (2.16)$$

$$G_{\varphi}(t, \mathbf{k}) \equiv \int_{\mathbf{x}} e^{-i\mathbf{k}\cdot\mathbf{x}} \langle \varphi(t, \mathbf{x}) \varphi(t, \mathbf{0}) \rangle. \quad (2.17)$$

Assuming that the Fourier transform is independent of the direction of \mathbf{k} , the actual power spectrum is defined by multiplying G_{φ} with the phase-space volume element,

$$\mathcal{P}_{\varphi}(t, k) \equiv \frac{k^3 G_{\varphi}(t, \mathbf{k})}{2\pi^2}. \quad (2.18)$$

The electric and magnetic power spectra, \mathcal{P}_E and \mathcal{P}_B , are defined analogously. We remark that in the non-Abelian case, the power spectra \mathcal{P}_E and \mathcal{P}_B are *not* gauge invariant as functions of k , as they involve correlating two different spatial positions (cf. eq. (2.17)). However, integrals over the power spectra are so, as they correspond to an equal-position correlator,

$$\langle \varphi(t, \mathbf{x}) \varphi(t, \mathbf{x}) \rangle = \int_0^\infty \frac{dk}{k} \mathcal{P}_{\varphi}(t, k). \quad (2.19)$$

To conclude this section, we note that all the fields in our system, and some of the parameters (κ, m), are dimensionful. In a numerical study, we need to express dimensionful quantities in units of some arbitrary scale. We choose for this role a length scale, denoted by ℓ . The scale should be set so that dimensionful parameters, and also initial conditions (cf. eq. (2.11)), are of order unity,

$$\tilde{\kappa} \stackrel{(2.3)}{\equiv} \frac{\kappa}{\ell} \sim 1, \quad \tilde{m} \stackrel{(2.10)}{\equiv} \ell m \equiv 1, \quad \ell^2 \dot{\varphi}(0) = \partial_{\tilde{t}} \tilde{\varphi}(0) \stackrel{(2.11)}{\sim} 1, \quad (2.20)$$

where the middle relation shows that in practice we have fixed ℓ in terms of the axion mass. Time and momentum are also rescaled, $\tilde{t} \equiv t/\ell$ and $\tilde{k} \equiv \ell k$. The same rescalings are applied on the lattice (cf. eqs. (B.35)–(B.37)). Keeping the lattice spacing small in these units, $\tilde{a} \equiv a/\ell \ll 1$, guarantees the absence of discretization artifacts.

3. Perturbative expectations

The system introduced in sec. 2 displays some well-known remarkable properties. Here, we recall the origin of the tachyonic instability, in order to compare it later with non-linear simulations (cf. sec. 5.3).

Let us consider a spatially homogeneous background value of φ , denoted by $\varphi(t, \mathbf{x}) \rightarrow \bar{\varphi}(t)$, like in eq. (2.11). We want to derive an equation of motion for \mathbf{B} in its presence, staying at linear order. Taking the curl of eq. (2.9), and making use of the Jacobi identities in eq. (2.6), yields

$$\ddot{\mathbf{B}} \stackrel{(2.6)}{\approx} \nabla^2 \mathbf{B} + \kappa \dot{\varphi} \nabla \times \mathbf{B}. \quad (3.1)$$

Going to momentum space in the spatial directions, and solving for the eigenvalues, the circular polarization states (\pm) evolve as

$$\ddot{B}_{k,\pm} \stackrel{(3.1)}{\approx} -k(k \pm \kappa \dot{\varphi}) B_{k,\pm}. \quad (3.2)$$

When $k < \kappa |\dot{\varphi}|_{\max}$, there is the possibility of exponential growth.

In order to solve eq. (3.2), we need initial conditions. Though we had set the initial magnetic field to vanish, a non-zero value is generated very rapidly through eq. (2.8), so in practice we can take a configuration carrying the same amount of energy density as the electric field in eq. (A.24), as given by eq. (A.25). The overall amplitude squared of the initial state is given by eq. (2.15). We let it phase-rotate according to the massless mode function,

$$B_{k,\pm}(0) = \sqrt{k f_k}, \quad \dot{B}_{k,\pm}(0) = -ik B_{k,\pm}(0). \quad (3.3)$$

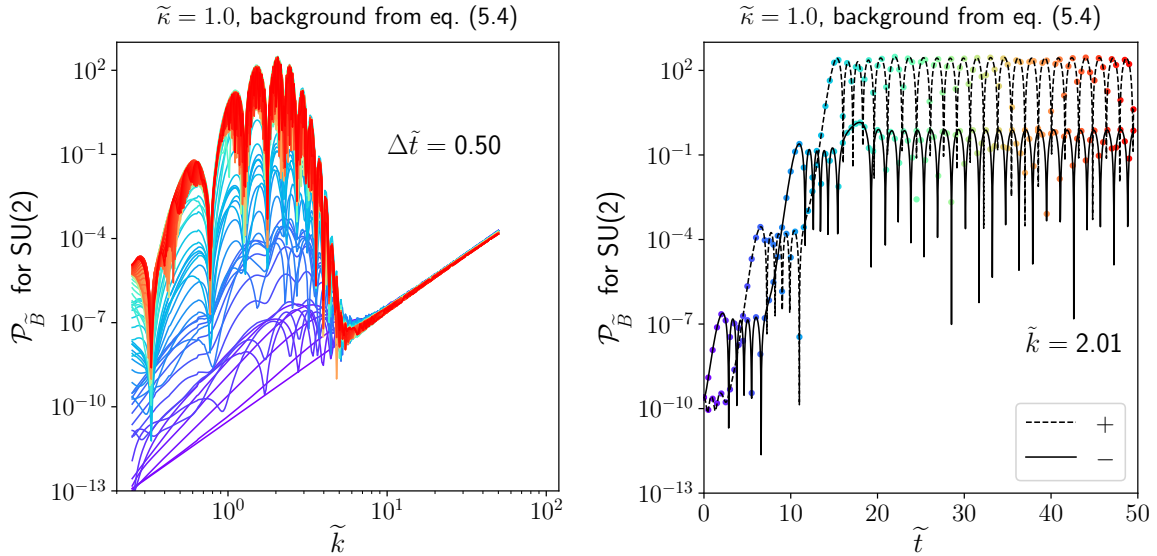


Figure 1: Left: A numerical solution of eq. (3.2), with initial conditions from eq. (3.3), background modelling from eq. (5.4), and the result plotted in terms of the power spectrum from eq. (3.4). The curves correspond to snapshots at equal time intervals, $\Delta\tilde{t} = 0.50$, and they display exponential growth for as long as $\dot{\varphi} \neq 0$ in eq. (3.2). As a function of \tilde{k} , they also show a band structure, characteristic of systems with periodically varying coefficients. The overall time period is the same as in fig. 6, however the linearized solution lacks the transfer of power to higher momenta that is seen there. Right: The time evolution of the positive and negative helicity modes, at fixed $\tilde{k} = 2.01$. The blobs correspond to the snapshots shown in the left panel (though there both helicities are summed together).

After rescaling to a dimensionless quantity \tilde{B} like in eq. (2.20), we plot the power spectrum

$$\mathcal{P}_{\tilde{B}} \stackrel{(2.18)}{\equiv} \stackrel{(B.35)}{\equiv} \frac{3\tilde{k}^3}{2\pi^2} [|\tilde{B}_{k,+}(\tilde{t})|^2 + |\tilde{B}_{k,-}(\tilde{t})|^2], \quad (3.4)$$

where the factor 3 counts the SU(2) generators.

For the condensate, we assume a form justified by our SU(2) simulation data, given in eq. (5.4). This function is time-antisymmetric in accordance with our initial conditions (cf. eq. (2.11)), and the coefficient $\tilde{\Upsilon} > 0$ accounts for the fact that oscillations decay after an unattenuated early time period, of duration \tilde{t}_0 . After fixing the parameters from a comparison with lattice data (cf. figs. 3–5), we show snapshots of the solution for $\mathcal{P}_{\tilde{B}}$ in fig. 1, taken at equal time intervals. For $\tilde{k} < \tilde{\kappa} |\dot{\tilde{\varphi}}|_{\max}$, there are bands of exponentially growing solutions. In the non-linear dynamics, we will see later on that the band structure gets smoothed by the interactions (cf. fig. 6), but exponential growth itself persists. It depletes the energy density in the axion condensate, and ultimately leads to the equipartition of the axion and gauge field energy densities (cf. fig. 7).

4. Numerical implementation

We now summarize the discretized version of sec. 2, with the details relegated to appendix B. The numerics has been implemented on the CosmoLattice platform [48, 49].

4.1. Spatial discretization

In order to study the dynamics numerically, we discretize the spatial directions with a lattice spacing, $a > 0$. While doing this, it is important to maintain gauge covariance. We achieve this by following the strategy of standard lattice gauge theories, in which the spatial gauge potentials, A_i^a , are replaced by unitary link matrices, $U_i \in \text{SU}(2)$, as the dynamical variables. The corresponding equations of motion are shown in eqs. (B.38)–(B.41). As demonstrated in appendix B.4, the time evolution of the spatially discretized equations conserves the total energy of the system exactly, as long as time is a continuous coordinate. Comparing with the physical length scale, ℓ (cf. eq. (2.20)), our default lattice spacing is

$$\tilde{a} \equiv \frac{a}{\ell} \approx 0.0332 . \quad (4.1)$$

4.2. Time discretization and finite-volume effects

In a simulation, the setup in eqs. (B.38)–(B.41) needs to be approximated in two further ways: by discretizing the time coordinate, and by placing the system in a finite volume.

As for the time coordinate, we choose a step $\delta\tilde{t} \ll \tilde{a}$, and solve the equations with a 3rd order Runge-Kutta algorithm [50, 51]. This algorithm is *not* symplectic, meaning that energy is not conserved exactly. However, by restricting to

$$\delta\tilde{t} \leq 0.15 \tilde{a} , \quad (4.2)$$

we find that energy is conserved up to relative accuracy 10^{-4} until times $\tilde{t} \leq 50$ for $\tilde{\kappa} \approx 2.0$, which is sufficient for our purposes. For smaller values of $\tilde{\kappa}$, a more accurate energy conservation is observed, and we can integrate up to later times.

As for the spatial volume, we adopt a cubic box of size N^3 , with periodic boundary conditions in all directions. Tests have been carried out with $N = 256, 512, 1024$, verifying the absence of significant volume dependence. Our $\text{SU}(2)$ production runs, whose results are reported in sec. 5, have been obtained with a fixed volume

$$N^3 = 756^3 . \quad (4.3)$$

The $\text{U}(1)$ production runs have identical parameters, except that the default volume is $N^3 = 512^3$. However, we have verified the volume-independence of our results at $N \geq 256$.

4.3. Initial conditions and power spectra

While we keep the initial conditions for the condensate fixed, cf. eq. (2.11), and make sure that it carries most of the initial energy density, we have tested various recipes for supplementing the condensate with noise. In the default setup, the noise for $\tilde{\varphi}$, which in continuum is given by eqs. (2.12)–(2.15), is implemented according to eqs. (B.56) and (B.57), respectively; the electric fields are initialized according to eq. (B.63); and the magnetic fields are set to zero, so as to satisfy the Gauss constraint from eqs. (B.19) and (B.20). In an alternative recipe, we put noise only in the magnetic fields (the links having been obtained from an exponential map of gauge potentials), setting $\tilde{\varphi}$ and \tilde{E}_i^a to zero. We have also tested cases where both electric and magnetic fields are initialized simultaneously, though then the Gauss constraint from eqs. (B.19) and (B.20) is not satisfied (it would be customary to “cool” the fields, in order to bring the violation of the Gauss constraint below a given tolerance, cf., e.g., refs. [45, 52, 53]). While there are quantitative differences between these choices, moderately impacting the fit value of $\tilde{\Upsilon}$ in the parameterization of eq. (5.4), the overall features of the equipartition dynamics stay the same. For our SU(2) production runs, reported in sec. 5, we use the default setup, with initial noise in $\tilde{\varphi}$ and \tilde{E}_i^a , but none in \tilde{B}_i^a .

Once the evolution starts, equal-time power spectra are measured in accordance with eqs. (2.17) and (2.18), as a function of time. In lattice units, the power spectra are given by eqs. (B.58) and (B.60).

5. Early stages of equilibration

Given the setup outlined in sec. 4, we proceed to the main results obtained from our simulations. For non-Abelian dynamics we consider the example of an SU(2) Yang-Mills theory, and compare throughout with the U(1) theory. As for the parameters, we have fixed

$$\tilde{m} \stackrel{(2.20)}{\equiv} 1, \quad g = 1.0, \quad \tilde{\kappa} = 0.2 \dots 2.0, \quad \partial_t \tilde{\varphi}(0) = 5.0. \quad (5.1)$$

The value of \tilde{m} represents a choice of the scaling factor, ℓ , and has no physical significance. The largish gauge coupling, $g = 1.0$, guarantees that non-Abelian interactions are fairly efficient. The physically most interesting variation is in $\tilde{\kappa}$, which parametrizes the strength of the interactions between the axion and gauge ensembles (cf. eq. (2.3)).

The results that we show are in general based on a single run in a large volume. When we take Fourier transforms, the smallest value shown is $\tilde{k} = 0.25$, corresponding to $\mathbf{n} = (1, 0, 0)$ in terms of eq. (B.54). For larger momenta, a single lattice volume contains several wavelengths, and effectively implements an ensemble average, as we have also explicitly verified by performing a few statistically independent runs.

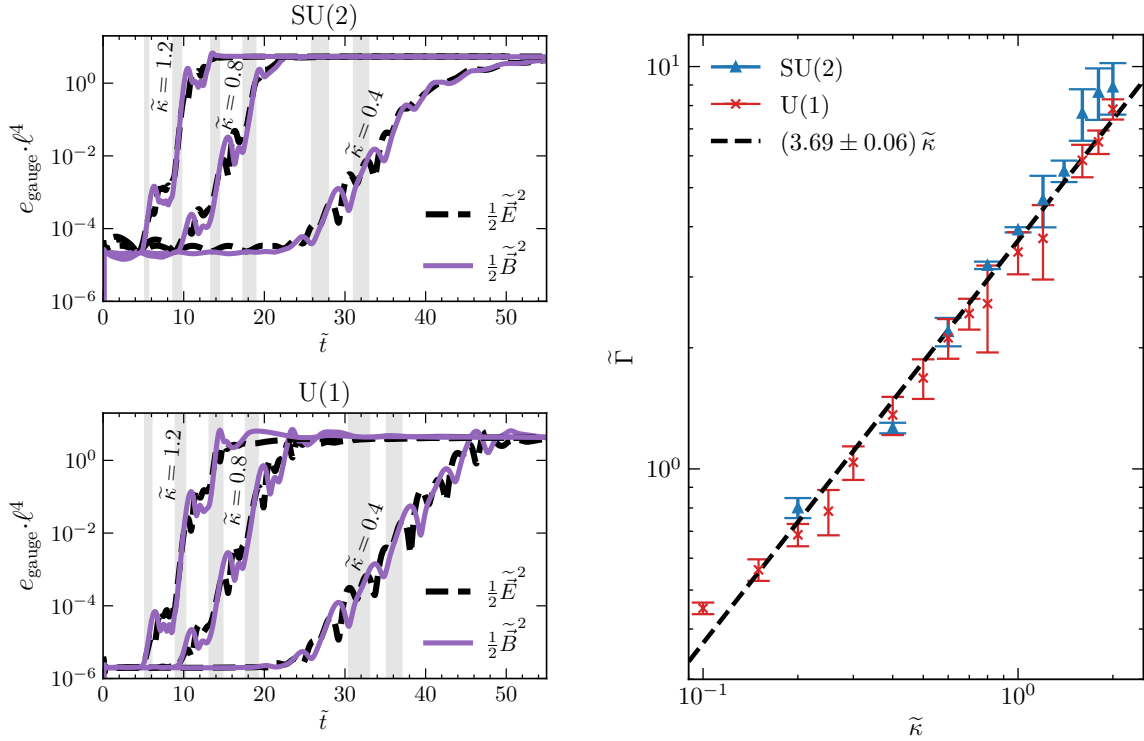


Figure 2: Left: Evolution of gauge-field energy densities as a function of time, \tilde{t} , for several $\tilde{\kappa}$, with the vector notation denoting a sum over both spatial and colour indices. The grey bands indicate domains of exponential growth. Right: The coefficient characterizing the exponential growth, $\tilde{\Gamma}$ (cf. eq. (5.2)), as a function of $\tilde{\kappa}$.

5.1. Exponential growth of gauge-field energy density

Linear perturbation theory, as explained around eq. (3.2), indicates that if $\tilde{\kappa} \dot{\tilde{\varphi}} \neq 0$, then IR modes with $\tilde{k} < \tilde{\kappa} |\dot{\tilde{\varphi}}|_{\text{max}}$ can experience exponential growth. The results of our numerical simulations validate this expectation. In fig. 2 we show the evolution of the energy densities in the electric and magnetic fields as a function of time, for several values of $\tilde{\kappa}$. The grey bands indicate regions of exponential growth. Between the grey bands, the growth ceases for a while; this corresponds to $|\dot{\tilde{\varphi}}|$ becoming smaller, so that the instability band becomes narrow. This general behaviour is in accordance with fig. 1. After having gone through a few instability bands, the gauge field energy density saturates; this takes longer for small $\tilde{\kappa}$, as the instability band is narrower. Then also the oscillations of $\tilde{\varphi}$ continue longer (cf. fig. 3).

In the grey bands of fig. 2, in which the relative growth rate of the gauge field energy density, $\dot{e}_{\text{gauge}}/e_{\text{gauge}}$, is approximately constant, we fit the behaviour to

$$e_{\text{gauge}}(\tilde{t}) \approx e_{\text{gauge},0} e^{\tilde{\Gamma} \Delta \tilde{t}}, \quad \Delta \tilde{t} \equiv \tilde{t} - \tilde{t}_0. \quad (5.2)$$

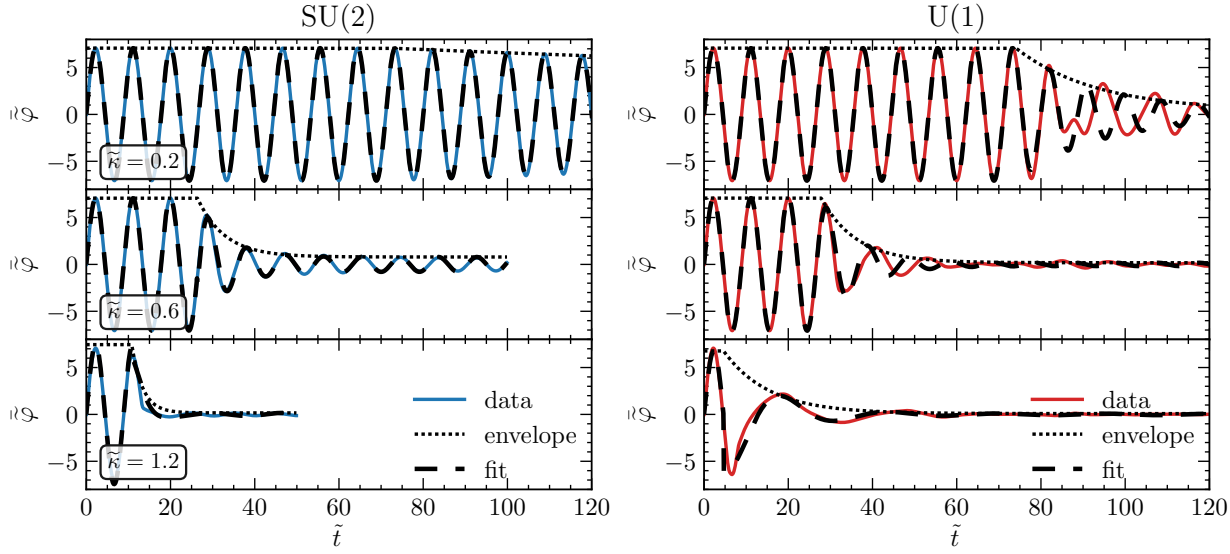


Figure 3: Illustration of axion oscillations and their subsequent damping, for SU(2) (left) and U(1) (right), for three representative values of $\tilde{\kappa}$. The dotted lines show a fit to the envelope of eq. (5.4), whereas the dashed lines represent a fit to the full eq. (5.4).

To obtain an uncertainty estimate for $\tilde{\Gamma}$, we average it over several bands. In the right panel of fig. 2, we plot $\tilde{\Gamma}$ as a function of $\tilde{\kappa}$ both for SU(2) and U(1). We observe an approximately linear dependence (dashed line), whose coefficient is remarkably similar in both cases.

5.2. Damping of axion oscillations

Turning to the axion field, from the measured data we extract the axion condensate through a spatial average,

$$\tilde{\varphi}(\tilde{t}) \equiv \frac{1}{N^3} \sum_{\mathbf{x}} \tilde{\varphi}(\tilde{t}, \mathbf{x}) . \quad (5.3)$$

Its evolution is shown in fig. 3, revealing a long period of oscillations for $\tilde{\kappa} \ll 1.0$, and an overdamped regime for $\tilde{\kappa} \gg 1.0$. Recalling fig. 2, the damping is due to a transfer of energy from the condensate to the gauge degrees of freedom (and to condensate fragmentation).

On a closer inspection, the pattern of damping is non-trivial, and only sets in after a while. In the SU(2) case we find that, as illustrated by the dashed lines in fig. 3 (left), the data can be well represented by

$$\tilde{\varphi}(\tilde{t}) \approx \begin{cases} \mathcal{A}_0 \sin(\tilde{\omega}_1 \tilde{t}), & \text{for } \tilde{t} < \tilde{t}_0, \\ \sin(\tilde{\omega}_2 \tilde{t} - \phi_2) \left\{ \exp\left(-\tilde{\Upsilon}(\tilde{t} - \tilde{t}_0)\right) (\mathcal{A}_0 - \mathcal{A}) + \mathcal{A} \right\}, & \text{for } \tilde{t} \geq \tilde{t}_0. \end{cases} \quad (5.4)$$

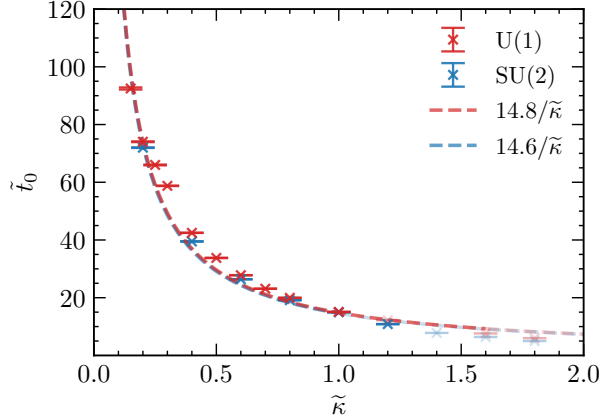


Figure 4: Illustration of the coefficient \tilde{t}_0 , characterizing the delay of when damping starts, as extracted from a fit to eq. (5.4). With a lighter shade we show points in the overdamped regime, where less than a full oscillation occurs before the damping sets in. In the latter regime, the error of the fitting procedure is significant.

Here, \mathcal{A}_0 and \mathcal{A} describe the initial and final oscillation amplitudes, respectively. The parameter \tilde{t}_0 describes the period of unattenuated oscillations, $\tilde{\omega}_1$ and $\tilde{\omega}_2$ the oscillation frequencies before and after the start of damping, and $\tilde{\Upsilon}$ the damping coefficient. The phase factor ϕ_2 is matched to guarantee continuity (the first derivative has a jump). The original oscillation frequency, $\tilde{\omega}_1$, is close but not equivalent to its tree-level value, \tilde{m} . We find that after the damping starts, the oscillations slow down, $\tilde{\omega}_2 < \tilde{\omega}_1$.

We interpret the delay parameter, \tilde{t}_0 , as originating from that the gauge modes need to grow to a critical threshold before allowing for a significant backreaction. As shown in fig. 3 (right), the delay is also present in U(1), but the subsequent damping is not well described by eq. (5.4). Hence, the physics leading to eq. (5.4) must reflect non-Abelian gauge self-interactions, for instance processes resembling sphaleron damping.

Let us take a closer look at \tilde{t}_0 . As shown in fig. 4, its dependence on $\tilde{\kappa}$ can be well represented by $\tilde{t}_0 \propto 1/\tilde{\kappa}$. The value of \tilde{t}_0 asymptotes to zero for large $\tilde{\kappa}$, though it must be added that as $\tilde{t}_0 \rightarrow 0$, less than a single undamped oscillation is present, which significantly increases the systematic uncertainty of our fitting routine. We indicate this by the lighter shading of these data points in our plot.

Turning to the axion damping coefficient, $\tilde{\Upsilon}$, shown in fig. 5, we find that a quadratic behaviour fits the SU(2) results for modest $\tilde{\kappa}$. This suggests that gauge fields are produced from the axion condensate at $\mathcal{O}(\tilde{\kappa})$, and backreact on it at $\mathcal{O}(\tilde{\kappa}^2)$. This is in analogy with sphaleron damping, which is also of $\mathcal{O}(\tilde{\kappa}^2)$.

However, when $\tilde{\kappa}$ is large, we enter the overdamped regime, where less than a single oscillation

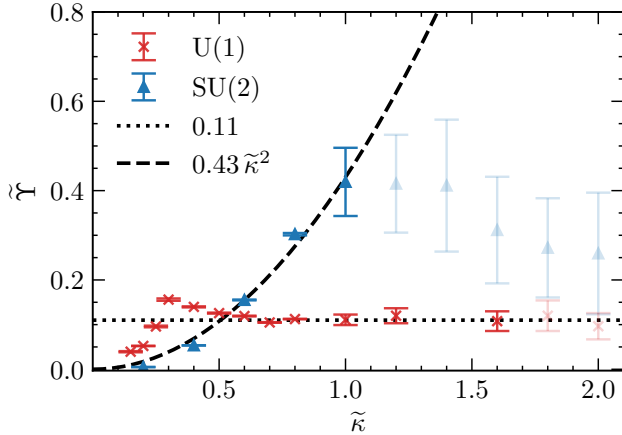


Figure 5: The axion damping coefficient $\tilde{\Upsilon}$, as extracted from a fit to eq. (5.4), for both SU(2) and U(1). We also illustrate possible quadratic and constant representations of the data. The points in the overdamped regime are shown with a lighter shade. Here less than a full oscillation takes place before the damping sets in, which significantly adds to the error of the fitting procedure.

is present. In this case there is an increased uncertainty associated with fitting \tilde{t}_0 and $\tilde{\Upsilon}$. To approximate the systematic error, we determine $\tilde{\Upsilon}$ for different fixed $\tilde{t}'_0 \in (\tilde{t}_0 - \pi/\tilde{m}, \tilde{t}_0 + \pi/\tilde{m})$. As visible in fig. 5 (points with lighter shade), the uncertainty soon becomes of order unity.

In the U(1) case, we observe first an increase of $\tilde{\Upsilon}$ with $\tilde{\kappa}$, and then a quick flattening to a constant value. In a different context, a similar flattening is observed in fig. 7. It is conceivable that the U(1) dynamics is dictated by the tachyonic instability, whereas in the SU(2) case, gauge-field self-interactions moderate the instability and thereby regulate the dynamics, leading to a “sequential” behaviour, associated with identifiable powers of $\tilde{\kappa}$.

5.3. Power spectra and energy equipartition

In analogy with eqs. (2.18) and (3.4), we define electric and the axion power spectra as

$$\mathcal{P}_{\tilde{E}} \equiv \frac{d_A \tilde{k}^3}{2\pi^2} [|\tilde{E}_{k,+}(\tilde{t})|^2 + |\tilde{E}_{k,-}(\tilde{t})|^2], \quad \mathcal{P}_{\tilde{\varphi}} \equiv \frac{\tilde{k}^3}{2\pi^2} |\tilde{\varphi}_k(\tilde{t})|^2, \quad (5.5)$$

where $d_A = 3 (1)$ denotes the number of generators of the gauge algebra, and $\tilde{E}_{k,\pm}$ and $\tilde{\varphi}_k$ are mode functions (if one uses Fourier transforms instead, the normalization contains an additional factor, cf. eq. (B.59)). In fig. 6 we show their time evolution for $\tilde{\kappa} = 1.0$, from an initial time $\tilde{t} = 0$ to a final time $\tilde{t} = 50$. Dark blue curves correspond to early times, dark red curves to late times. The sharp cutoff of the initial spectrum is due to the imposed momentum cutoff Λ in eq. (2.15).

The power spectra show initial growth in the instability band $\tilde{k} < \tilde{\kappa}|\dot{\tilde{\varphi}}|_{\max}$, indicated with

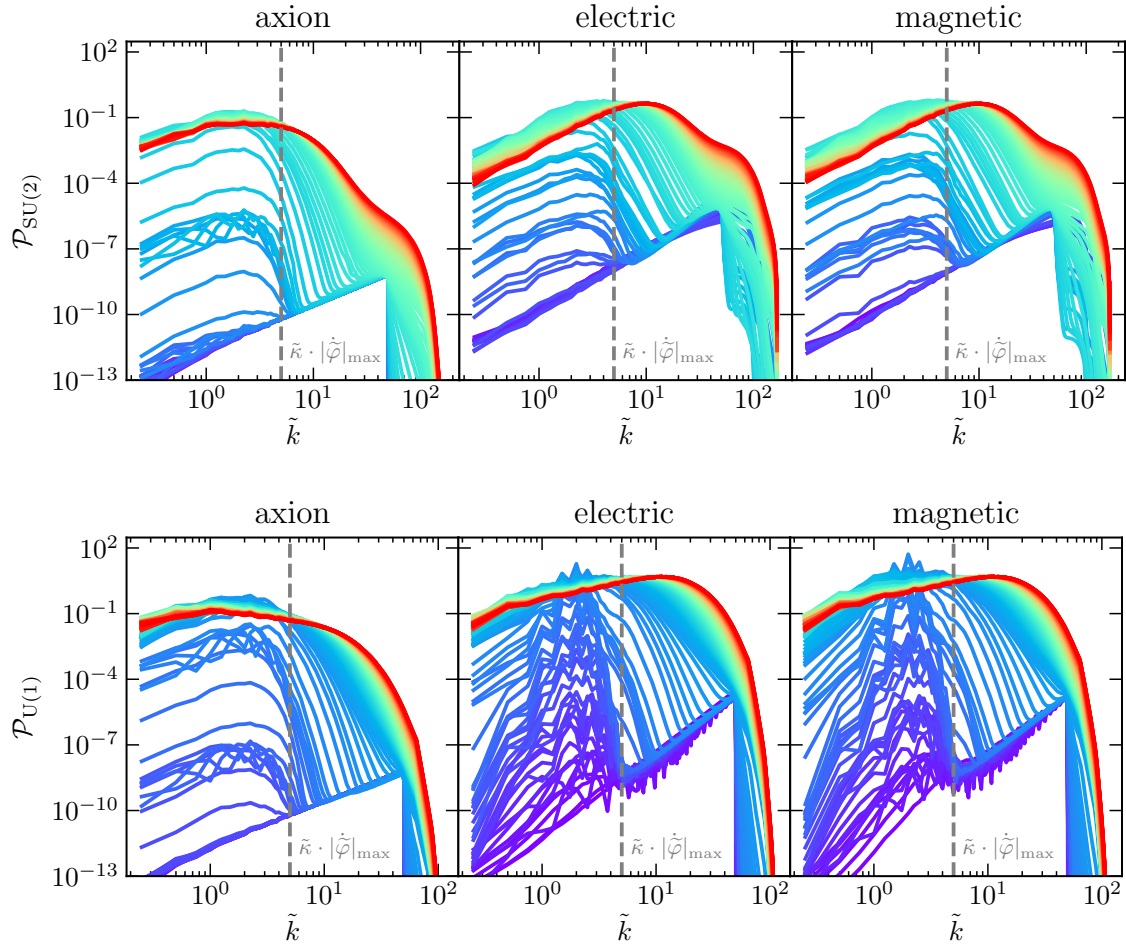


Figure 6: Top panels: Time evolutions of the SU(2) power spectra for $\tilde{\varphi}$, \tilde{E} , and \tilde{B} , for $\tilde{\kappa} = 1.0$, at time intervals $\Delta\tilde{t} = 0.5$. Bottom panels: The same for U(1). On the qualitative level, the right panels can be compared with the linearized expectations from fig. 1.

the dashed vertical lines. Subsequently energy gets transferred to higher-momentum modes. The process is noticeably smoother in SU(2) (top panels) than in U(1) (bottom panels), with the latter displaying oscillatory features reminiscent of fig. 1. We interpret the smoothening of the SU(2) power spectra as originating from the gauge self-interactions present in that case. However, there are interactions also in the U(1) case, mediated by the axions. Therefore, in both cases, energy is ultimately transferred also outside of the instability band. In fact, in the end, much of the power lies in the UV modes, which in the classical lattice theory reflect dispersion relations of the Brillouin zone.

In the left panels of fig. 7, we quantify energy equipartition between the gauge and axion sectors, as a function of time, for two values of the coupling strength $\tilde{\kappa}$. For SU(2), where the

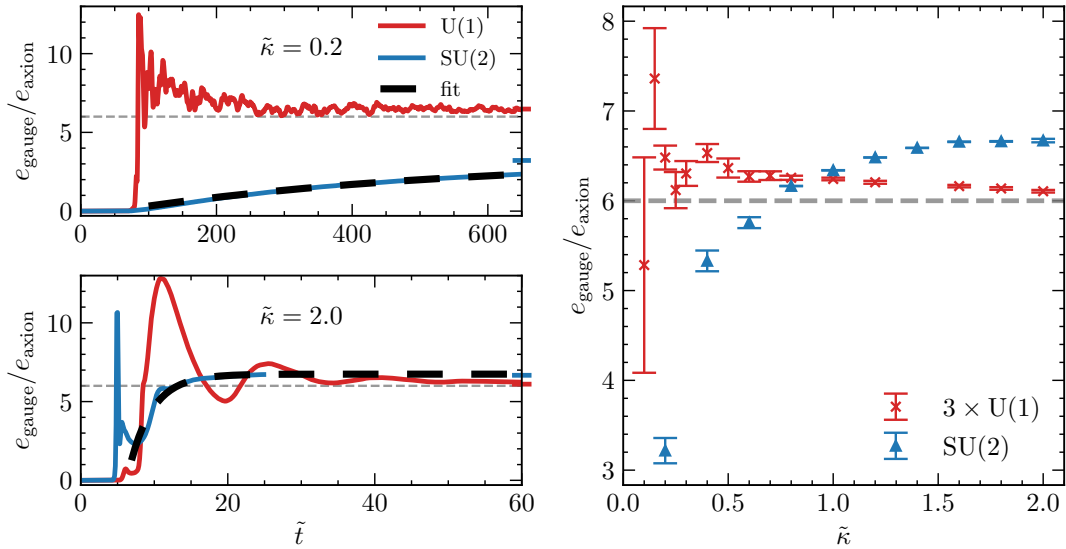


Figure 7: Left: The time evolution of the ratio of the gauge and axion energy densities, for small and large $\tilde{\kappa}$. The U(1) results have been multiplied by a factor 3. For small $\tilde{\kappa}$, the energy transfer to the gauge sector is much faster for U(1), due to the tachyonic instability. For SU(2), the dashed lines show an exponential fit to late times. The asymptotic late-time values are indicated with short blocks along the right vertical axis. Right: The late-time values as a function of $\tilde{\kappa}$.

energy transfer is fairly slow for small $\tilde{\kappa}$, the estimate for the asymptotic value is obtained from an exponential fit at finite times. For U(1), the process is much faster, and the asymptotic value is estimated by taking an average over oscillations at late times.

The asymptotic energy densities are shown in the right panel of fig. 7, where we have summed over the electric and magnetic contributions. The U(1) results have been multiplied by a factor 3, to make them easily comparable with the SU(2) results.

For SU(2), we observe a smooth dependence on $\tilde{\kappa}$, with the $\tilde{\kappa} \rightarrow 0$ limit decreasing, and the large- $\tilde{\kappa}$ limit overshooting the expected value of 6 by $\sim 10\%$. The value 6 corresponds to a non-interacting continuum estimate, accounting for the two degrees of freedom per each of the three gauge bosons, divided by the one degree of freedom of the axion. The deviation from 6 originates likely from interactions, which modify both the axion and the gauge-field energy densities.

In contrast, in the U(1) case, the dependence on $\tilde{\kappa}$ is *not* smooth, but the energy is efficiently transferred to the gauge sector as soon as $\tilde{\kappa} \neq 0$. The efficient transfer likely reflects the tachyonic instability. The ratio equals 2, accounting for two degrees of freedom of the photon divided by one degree of freedom of the axion, up to a correction of $\sim 3\%$. The relative deviation from the free value is smaller than for SU(2), likely due to the absence of

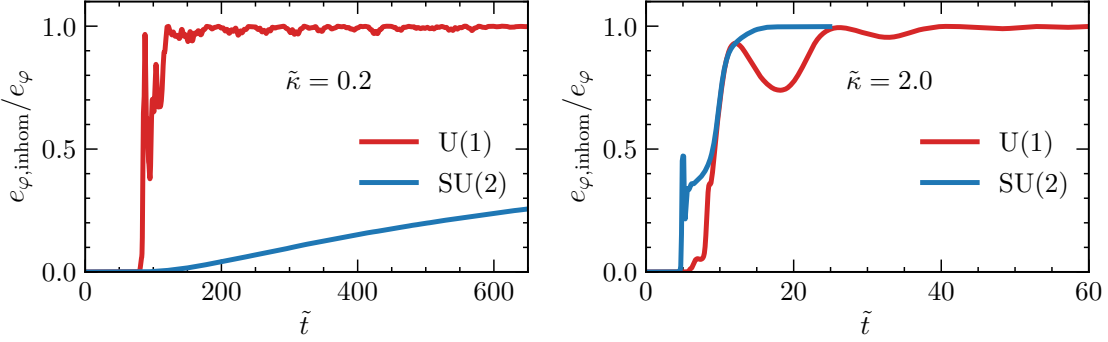


Figure 8: The fraction of axion energy density in inhomogeneous fluctuations, for $\tilde{\kappa} = 0.2$ (left) and $\tilde{\kappa} = 2.0$ (right). Comparing with fig. 7, the transfer of energy to axion inhomogeneities happens approximately simultaneously with the transfer of energy to the gauge sector.

self-interactions in the gauge sector.

Finally, in fig. 8, we show the fraction of the axion energy density that is contained in inhomogeneous fluctuations, after subtracting the contribution from the condensate, as defined in eq. (5.3), such that

$$\tilde{\varphi}_{\text{inhom}}(\tilde{t}, \mathbf{x}) \equiv \tilde{\varphi}(\tilde{t}, \mathbf{x}) - \bar{\varphi}(\tilde{t}), \quad (5.6)$$

$$\tilde{e}_{\varphi, \text{inhom}}(\tilde{t}, \mathbf{x}) \equiv \frac{1}{2} \dot{\tilde{\varphi}}_{\text{inhom}}^2(\tilde{t}, \mathbf{x}) + \frac{1}{2} |\nabla \tilde{\varphi}_{\text{inhom}}(\tilde{t}, \mathbf{x})|^2 + \frac{1}{2} \tilde{m}^2 \tilde{\varphi}_{\text{inhom}}^2(\tilde{t}, \mathbf{x}). \quad (5.7)$$

If we interpret the transfer of energy to the gauge sector as a prerequisite for the latter to equilibrate, then this plot shows that the axion field has a chance to equilibrate about as fast as the gauge plasma. However, we remark that from the point of view of warm inflation, the equilibration of the gauge plasma is the more important phenomenon, as the gauge plasma dominates the radiation energy density and generates the sphaleron friction.

6. Conclusions and outlook

The purpose of this paper has been to initiate the numerical study of how an axion-like inflaton field (φ) and a non-Abelian gauge ensemble interact with each other. To this aim, we have varied the dimensionless coupling characterizing the strength of the interaction, $\tilde{\kappa} = \alpha m / (2\pi f_a)$ (cf. eqs. (2.3) and (2.20)), in the range $\tilde{\kappa} = 0.2, \dots, 2.0$, and simulated the system on a lattice of size 756^3 . Most of the initial energy density is carried by a spatially homogeneous φ -condensate. Adding a tiny amount of noise switches on the decay channel to the gauge ensemble, and the energy density of the condensate gets rapidly transferred to other degrees of freedom (gauge fluctuations and spatial variations of φ).

The dynamics that we observe for SU(2) displays smooth parametric dependences, characteristics of a linear-response regime. The energy density in the electric and magnetic fields grows exponentially in time, with a growth rate approximately linearly proportional to $\tilde{\kappa}$,

$$\tilde{\Gamma} \stackrel{\text{fig. 2}}{\approx} 3.7 \tilde{\kappa} \stackrel{(2.20)}{\Rightarrow} \Gamma \approx 3.7 m^2 \kappa. \quad (6.1)$$

Axion oscillations get damped, and in the SU(2) case, the damping rate is approximately quadratic in $\tilde{\kappa}$,

$$\tilde{\Upsilon} \stackrel{\text{fig. 5}}{\approx} 0.4 \tilde{\kappa}^2 \stackrel{(2.20)}{\Rightarrow} \Upsilon \approx 0.4 m^3 \kappa^2. \quad (6.2)$$

However, axion damping only sets in after a while, once the gauge ensemble has obtained a sufficient energy density, and this delay factor scales as

$$\tilde{t}_0^{-1} \stackrel{\text{fig. 4}}{\approx} 0.07 \tilde{\kappa} \stackrel{(2.20)}{\Rightarrow} t_0^{-1} \approx 0.07 m^2 \kappa. \quad (6.3)$$

The delay may be sensitive to the amount of noise that we inserted in the initial state, and therefore not an equally important physical characteristic of the system as Γ and Υ . In the end, the overall energy density in the gauge sector is about $2(N_c^2 - 1)$ times larger than that in the axion field, manifesting energy equipartition (cf. fig. 7).

Physically, it would be tempting to identify the energy equipartition that we observe with equilibration (or thermalization). However, strictly speaking the latter phenomenon cannot be studied with classical lattice gauge theory, because the thermal momentum scale, $k \sim T$, has been replaced by the unphysical lattice cutoff scale, $k \sim \pi/a$. Nevertheless, given that overall energy is conserved and the Hubble rate vanishes, the physical analogue of our setup corresponds to *instantaneous reheating*, in which all of the condensate energy density gets ultimately transferred to equipartitioned UV degrees of freedom.

Turning to a comparison with the U(1) case, we note that even though it does display many similarities with SU(2), we have also shown that there is a very marked difference. In U(1), the dependence on κ is not smooth, but even a small non-zero value leads to rapid equipartition (cf. fig. 7). We suspect that this is due to the tachyonic instability, which is not much attenuated in the absence of gauge-field self-interactions.

For the present study, we have kept the non-Abelian gauge coupling fixed, $g^2 = 1.0$. In principle, it would be interesting to vary the strength of the gauge self-interaction, while keeping κ fixed. Unfortunately it is not entirely trivial to do this in the classical theory, due to its scale invariance.¹ Nevertheless, it would be interesting to explore how this variation could be implemented in a physically meaningful way.

¹The evolution equations, (B.38)–(B.41), are invariant under the simultaneous change $g \rightarrow x g$, $\tilde{\kappa} \rightarrow x \tilde{\kappa}$, $\tilde{\varphi} \rightarrow \tilde{\varphi}/x$, $\tilde{E}_i^a \rightarrow \tilde{E}_i^a/x$, and $\tilde{B}_i^a \rightarrow \tilde{B}_i^a/x$. Therefore any change of g can be compensated for by a change of $\tilde{\kappa}$ and a rescaling of initial conditions.

A second important next step is to include the expansion of the universe in the simulations. The expansion option is built in into the CosmoLattice platform [48, 49], so we hope to return to this topic in the foreseeable future.

Finally, the inclusion of fermions represents another interesting avenue. Even if elementary fermions do not permit for a classical description, an ensemble average over fermions can indeed be included, via a time-dependent chemical potential, which can bias sphaleron processes. We leave this extension to an upcoming study.

Acknowledgements

KB thanks the U.S. Department of Energy, Office of Science, Office of High Energy Physics, under Award Number DE-SC0011632, and the Walter Burke Institute for Theoretical Physics. Test runs for this work were conducted at the Resnick High Performance Computing Center, a facility supported by Resnick Sustainability Institute at the California Institute of Technology. AF and FRS are supported by the Deutsche Forschungsgemeinschaft (DFG, German Research Foundation) through the Emmy Noether Programme Project No. 545261797, and the CRC-TRR 211 "Strong-interaction matter under extreme conditions," Project No. 315477589-TRR 211. The authors gratefully acknowledge the computing time made available to them on the high-performance computer Noctua 2 at the NHR Paderborn Center for Parallel Computing (PC2). This center is jointly supported by the Federal Ministry of Research, Technology and Space and the state governments participating in the National High-Performance Computing (NHR) joint funding program (www.nhr-verein.de/en/our-partners).

A. Equations of motion in continuum

Though well known, we specify here the continuum evolution equations and initial conditions that our study corresponds to. For ease of reference, the discussion is structured identically to appendix B, where the technically more involved discretized setup is introduced.

Notation. It is convenient to define a covariant derivative as $D_\mu \equiv \partial_\mu + igT^a A_\mu^a$, given that this removes unnecessary minus signs from the lattice formulation (cf., e.g., eqs. (B.10)–(B.12)). Here T^a are the generators of $SU(N_c)$, normalized as $\text{Tr}(T^a T^b) = \delta^{ab}/2$. Then the components of the field strength, $F_{\mu\nu} \equiv T^a F_{\mu\nu}^a = [D_\mu, D_\nu]/(ig)$, can be written as

$$F_{\mu\nu}^a = \partial_\mu A_\nu^a - \mathcal{D}_\nu^{ac} A_\mu^c, \quad (\text{A.1})$$

where $\mathcal{D}_\nu^{ac} \equiv \delta^{ac} \partial_\nu - g f^{abc} A_\nu^b$ is the covariant derivative in the adjoint representation.

We express the components of the field strength as

$$F_{0i}^a \stackrel{(\text{A.1})}{=} \underbrace{\dot{A}_i^a}_{\equiv E_i^a} - \mathcal{D}_i^{ac} A_0^c, \quad F_{ij}^a \equiv \epsilon_{ijk} B_k^a. \quad (\text{A.2})$$

This defines the electric and magnetic fields that we make use of in the following. We note that when $\kappa \neq 0$ (cf. eq. (2.3)), the electric field does *not* correspond to a canonical momentum.

Making use of $\epsilon^{0ijk} = \epsilon_{ijk}$, the Lagrangian, $L = \int_{\mathbf{x}} \mathcal{L}$, where \mathcal{L} is from eq. (2.1), can be written as

$$L \stackrel{(2.1)}{=} \int_{\mathbf{x}} \left\{ \frac{1}{2} \dot{\varphi}^2 - \frac{1}{2} \partial_i \varphi \partial_i \varphi - V(\varphi) + \frac{1}{2} F_{0i}^a F_{0i}^a - \frac{1}{4} F_{ij}^a F_{ij}^a - \kappa \varphi F_{0i}^a B_i^a \right\}. \quad (\text{A.3})$$

Gauss constraint and Hamiltonian. Given that the Lagrangian in eq. (A.3) does not depend on \dot{A}_0^a , the corresponding Euler-Lagrange equation states that

$$0 = \frac{d}{dt} \frac{\delta L}{\delta \dot{A}_0^a(x)} = \frac{\delta L}{\delta A_0^a(x)}, \quad x \equiv (t, \mathbf{x}). \quad (\text{A.4})$$

Subsequently, we choose the temporal gauge, $A_0^a(x) = 0 \quad \forall a, x$. The field A_0^a appears in eq. (A.3) only through the field strength F_{0i}^a , cf. eq. (A.2). Thus,

$$0 = G(x) \equiv T^a \frac{\delta L}{\delta A_0^a(x)} \Big|_{A_0^a=0} = T^a \left[\mathcal{D}_i^{ac} E_i^c - \kappa \mathcal{D}_i^{ac} (\varphi B_i^c) \right]. \quad (\text{A.5})$$

Making use of the Jacobi identity

$$T^a \mathcal{D}_i^{ac} B_i^c = \epsilon_{ikm} [D_i, [D_k, D_m]]/(2ig) = 0, \quad (\text{A.6})$$

which implies that \mathcal{D}_i^{ac} only acts on φ in eq. (A.5), leads to the Gauss constraint, which is given in eq. (2.5). The Jacobi identity itself is expressed more concisely through eq. (2.6).

Apart from the Lagrangian, we are interested in the total energy of the system. We refer to this as the *Hamiltonian*, H , even though we do *not* re-express the time derivatives (“ \dot{q} ”) in terms of canonical momenta (“ p ”).

The Hamiltonian is obtained with a Legendre transform from the Lagrangian:

$$H = \int_{\mathbf{x}} \left[\dot{\varphi}(x) \frac{\delta L|_{A_0^a=0}}{\delta \dot{\varphi}(x)} + E_i^a(x) \frac{\delta L|_{A_0^a=0}}{\delta E_i^a(x)} \right] - L|_{A_0^a=0}. \quad (\text{A.7})$$

The axion-gauge coupling drops out in this transformation, and we obtain

$$H \stackrel{(\text{A.3})}{\substack{(\text{A.7})}} \int_{\mathbf{x}} \left\{ \frac{1}{2} \dot{\varphi}^2 + \frac{1}{2} \partial_i \varphi \partial_i \varphi + V(\varphi) + \frac{1}{2} E_i^a E_i^a + \frac{1}{4} F_{ij}^a F_{ij}^a \right\}. \quad (\text{A.8})$$

Evolution equations. After having fixed $A_0^a = 0$ and taken care of the consistency of this procedure through the Gauss constraint, the remaining Euler-Lagrange equations read

$$\partial_t \left(\frac{\delta L|_{A_0^a=0}}{\delta \dot{\varphi}(x)} \right) = \frac{\delta L|_{A_0^a=0}}{\delta \varphi(x)}, \quad \partial_t \left(\frac{\delta L|_{A_0^a=0}}{\delta E_i^a(x)} \right) = \frac{\delta L|_{A_0^a=0}}{\delta A_i^a(x)} \quad \forall i, a, x. \quad (\text{A.9})$$

From eq. (A.3), the derivative with respect to E_i^a yields

$$\frac{\delta L|_{A_0^a=0}}{\delta E_i^a(x)} \stackrel{(\text{A.3})}{=} E_i^a - \kappa \varphi B_i^a. \quad (\text{A.10})$$

For the derivative with respect to A_i^a , we note that

$$\frac{\delta}{\delta A_i^a(x)} \int_{\mathbf{y}} F_{jk}^b f(y) = (\delta_{i,j} \mathcal{D}_k^{ab} - \delta_{i,k} \mathcal{D}_j^{ab}) f(x). \quad (\text{A.11})$$

This gives

$$\frac{\delta L|_{A_0^a=0}}{\delta A_i^a(x)} \stackrel{(\text{A.3})}{\substack{(\text{A.11})}} -\mathcal{D}_k^{ac} F_{ik}^c - \kappa \epsilon_{ikj} \mathcal{D}_k^{ac} (\varphi E_j^c) = -[\mathcal{D} \times \mathbf{B} + \kappa \mathcal{D} \times (\varphi \mathbf{E})]_i^a. \quad (\text{A.12})$$

When combining eqs. (A.10) and (A.12) according to eq. (A.9), we can furthermore make use of the Jacobi identity

$$\epsilon^{n\mu\nu\rho} [D_\mu, [D_\nu, D_\rho]] = 0 \quad \forall n \in \{1, 2, 3\}. \quad (\text{A.13})$$

Noting that one among the indices μ, ν, ρ is necessarily time, and rewriting the identity with the \mathbf{B} and \mathbf{E} fields, this implies the second relation given in eq. (2.6).

With the help of eq. (2.6), we note that $\dot{\mathbf{B}}$ from the time derivative of eq. (A.10) and $\mathcal{D} \times \mathbf{E}$ from eq. (A.12) cancel each other. To summarize, the equations of motion obtained from the $A_0^a = 0$ gauging of eq. (A.3) can be expressed as

$$\ddot{\varphi} \stackrel{(\text{A.3})}{\substack{(\text{A.9})}} \nabla^2 \varphi - V'(\varphi) - \kappa \mathbf{E} \cdot \mathbf{B}, \quad (\text{A.14})$$

$$\dot{\mathbf{A}} \stackrel{(\text{A.2})}{=} \mathbf{E}, \quad (\text{A.15})$$

$$\dot{\mathbf{E}} \stackrel{(\text{A.10}), (\text{A.12})}{\substack{(\text{2.6}), (\text{A.9})}} -\mathcal{D} \times \mathbf{B} + \kappa (\dot{\varphi} \mathbf{B} - \nabla \varphi \times \mathbf{E}). \quad (\text{A.16})$$

Energy conservation. A useful crosscheck of the equations of motion is that the total energy from eq. (A.8) remains conserved. Expressing F_{ij}^a in terms of B_k^a , we obtain

$$\begin{aligned} \dot{H} &\stackrel{(A.8)}{=} \int_{\mathbf{x}} \left\{ \dot{\varphi} \left[\underbrace{\ddot{\varphi}}_{(A.14)} + V'(\varphi) \right] + \partial_i \varphi \partial_i \dot{\varphi} + E_i^a \underbrace{\dot{E}_i^a}_{(A.16)} + B_i^a \underbrace{\dot{B}_i^a}_{(2.6)} \right\} \\ &= \int_{\mathbf{x}} \left\{ \partial_i (\dot{\varphi} \partial_i \varphi) \underbrace{- \mathbf{E} \cdot \mathcal{D} \times \mathbf{B} + \mathbf{B} \cdot \mathcal{D} \times \mathbf{E}}_{\epsilon_{ijk} \partial_i (E_j^a B_k^a)} - \underbrace{\kappa \mathbf{E} \cdot \nabla \varphi \times \mathbf{E}}_{0 \text{ by antisymmetry}} \right\}. \end{aligned} \quad (A.17)$$

The integrand is a total derivative, so \dot{H} vanishes if we assume periodic boundary conditions for gauge-invariant quantities.

Conservation of Gauss constraint. A final crosscheck is offered by that the Gauss constraint from eq. (2.5) is time-translation invariant at every position \mathbf{x} . Writing the spatial indices explicitly, we get

$$\begin{aligned} \dot{G} &\stackrel{(2.5)}{=} ig \underbrace{[\dot{A}_i, E_i]}_0 + \underbrace{[D_i, \dot{E}_i]}_{\text{insert (A.16)}} - \kappa \dot{\varphi}_{,i} B_i - \kappa \varphi_{,i} \dot{B}_i \\ &= - \underbrace{\frac{\epsilon_{ijk} \epsilon_{kmn}}{2} [D_i, [D_j, [D_m, D_n]]]}_{=0} \\ &\quad + \kappa \left\{ \dot{\varphi} \underbrace{[D_i, B_i]}_{(2.6) \equiv 0} - \underbrace{\epsilon_{ijk} \varphi_{,ij}}_{i \leftrightarrow j} E_k + \varphi_{,i} \underbrace{(\epsilon_{ijk} [D_j, E_k] - \dot{B}_i)}_{(2.6) \equiv 0} \right\} = 0. \end{aligned} \quad (A.18)$$

The conservation of the Gauss constraint is a consequence of many non-trivial cancellations, and therefore offers for a strong crosscheck.

Initial conditions and power spectra. Even though our evolution equations are classical, we can try to mimick quantum-mechanical effects through initial conditions [44]. Let us first recall that if φ were a quantum field, denoted by $\hat{\varphi}$, it could be expressed in a mode expansion as

$$\hat{\varphi}(x) = \int_{\mathbf{k}} \left[\hat{a}_{\mathbf{k}} \varphi_k(t) e^{i\mathbf{k} \cdot \mathbf{x}} + \hat{a}_{\mathbf{k}}^\dagger \varphi_k^*(t) e^{-i\mathbf{k} \cdot \mathbf{x}} \right], \quad \int_{\mathbf{k}} \equiv \int \frac{d^3 \mathbf{k}}{(2\pi)^3}, \quad (A.19)$$

where the canonical commutation relations and the mode function read

$$[\hat{a}_{\mathbf{k}}, \hat{a}_{\mathbf{q}}^\dagger] = (2\pi)^3 \delta^{(3)}(\mathbf{k} - \mathbf{q}), \quad \varphi_k(t) = \frac{e^{-i\omega_k t}}{\sqrt{2\omega_k}}, \quad \omega_k \equiv \sqrt{k^2 + m^2}. \quad (A.20)$$

Computing the equal-time 2-point function in a non-interacting (“Bunch-Davies”) vacuum yields

$$\langle 0 | \hat{\varphi}(t, \mathbf{x}) \hat{\varphi}(t, \mathbf{y}) | 0 \rangle \stackrel{(A.19)}{=} \int_{\mathbf{k}} e^{i\mathbf{k} \cdot (\mathbf{x} - \mathbf{y})} |\varphi_k(t)|^2. \quad (A.21)$$

A quantum-mechanical *power spectrum* is defined by multiplying the integrand of eq. (A.21) with the phase-space volume element,

$$\mathcal{P}_\varphi(t, k) \equiv \frac{k^3}{2\pi^2} |\varphi_k(t)|^2. \quad (\text{A.22})$$

In the classical theory, we write down an expansion like in eq. (A.19), but replace the creation and annihilation operators by complex random variables, $c_{\mathbf{k}}$ and $c_{\mathbf{k}}^*$. This leads to the expressions shown in eqs. (2.12) and (2.13). Computing the 2-point function, we get a contribution from two terms, $\langle c_{\mathbf{k}} c_{\mathbf{q}}^* \rangle$ and $\langle c_{\mathbf{k}}^* c_{\mathbf{q}} \rangle$. There is no analogue for the latter in the quantum theory, given that $\hat{a}_{\mathbf{q}}|0\rangle = 0$. To compensate for this, and thereby to reproduce classically the results in eqs. (A.21) and (A.22), we should multiply the classical noise autocorrelator by the factor f_k , as shown in eq. (2.14). However, in the present study, we have reduced the quantum noise to an even lower level, according to eq. (2.15).

For the gauge sector, we envisage a gauge potential similar to that in eq. (2.12),

$$\mathbf{A}(t, \mathbf{x}) = \int_{\mathbf{k}} \sum_{\lambda=\pm} \left[c_{\mathbf{k}} \mathbf{e}_{\mathbf{k}}^\lambda \chi_k(t) e^{i\mathbf{k}\cdot\mathbf{x}} + c_{\mathbf{k}}^* \mathbf{e}_{\mathbf{k}}^{\lambda*} \chi_k^*(t) e^{-i\mathbf{k}\cdot\mathbf{x}} \right], \quad (\text{A.23})$$

where the (circular) polarization vectors satisfy $\mathbf{k} \times \mathbf{e}_{\mathbf{k}}^\pm = \pm ik \mathbf{e}_{\mathbf{k}}^\pm$, and the mode function is like in eq. (A.20) but with zero mass, $\chi_k(t) \equiv e^{-ikt}/\sqrt{2k}$. Via eq. (A.15), we then obtain an initial value for the electric field, similar to eq. (2.12),

$$\mathbf{E}(0, \mathbf{x}) = \int_{\mathbf{k}} \sum_{\lambda=\pm} (ik) \left[-c_{\mathbf{k}} \mathbf{e}_{\mathbf{k}}^\lambda \chi_k(0) e^{i\mathbf{k}\cdot\mathbf{x}} + c_{\mathbf{k}}^* \mathbf{e}_{\mathbf{k}}^{\lambda*} \chi_k^*(0) e^{-i\mathbf{k}\cdot\mathbf{x}} \right]. \quad (\text{A.24})$$

For the magnetic field, in a free limit we would similarly get

$$\mathbf{B}(0, \mathbf{x}) \stackrel{\text{free}}{\approx} \int_{\mathbf{k}} \sum_{\lambda=\pm} (ik) \times \left[c_{\mathbf{k}} \mathbf{e}_{\mathbf{k}}^\lambda \chi_k(0) e^{i\mathbf{k}\cdot\mathbf{x}} - c_{\mathbf{k}}^* \mathbf{e}_{\mathbf{k}}^{\lambda*} \chi_k^*(0) e^{-i\mathbf{k}\cdot\mathbf{x}} \right]. \quad (\text{A.25})$$

However, as discussed in sec. 4.3, in our default setup we set $\mathbf{B}(0, \mathbf{x}) = \mathbf{0}$ in order to satisfy the Gauss constraint, though a non-zero value is generated very rapidly by the dynamics.

B. Equations of motion on a spatial lattice

Following the derivation of the continuum equations in appendix A, we transcribe them here to spatial discretization. The lattice spacing is denoted by a . The discretization is not unique; we implement it in a simple way, respecting gauge invariance, and comment on possibilities for “improvement” along the way.

B.1. Notation and canonical coordinates

The basic variables of the lattice theory are the scalar field $\varphi(x)$, which lives on the sites x ; the group elements $U_i(x)$, which live on the links between x and $x + a\mathbf{i}$; and the temporal field component $A_0(x)$, which lives on the sites. With these degrees of freedom, the $0i$ -component of a field strength tensor is written in a form analogous to eq. (A.1),

$$\widehat{F}_{0i}(x) \equiv \frac{1}{iag} [\dot{U}_i(x)] U_i^\dagger(x) + \frac{A_0(x) - U_i(x) A_0(x + a\mathbf{i}) U_i^\dagger(x)}{a}. \quad (\text{B.1})$$

It can be verified that under a gauge transformation, $\Omega(x) \in \text{SU}(N_c)$, defined as

$$U'_i(x) \equiv \Omega(x) U_i(x) \Omega^\dagger(x + a\mathbf{i}), \quad A'_0(x) \equiv \Omega(x) A_0(x) \Omega^\dagger(x) + \frac{1}{ig} \Omega(x) \dot{\Omega}^\dagger(x), \quad (\text{B.2})$$

the field strength transforms covariantly, $\widehat{F}_{0i}(x) \rightarrow \Omega(x) \widehat{F}_{0i}(x) \Omega^\dagger(x)$.

The spatial components of the field strength are discretized by making use of a plaquette,

$$P_{ij}(x) \equiv U_i(x) U_j(x + a\mathbf{i}) U_i^\dagger(x + a\mathbf{j}) U_j^\dagger(x), \quad P_{ji} = P_{ij}^\dagger. \quad (\text{B.3})$$

In the naive continuum limit, the plaquette can be represented as $P_{ij}(x) \simeq e^{ia^2 g F_{ij}}$, and therefore the term appearing in the Lagrangian is defined as

$$\frac{\widehat{F}_{ij}^a \widehat{F}_{ij}^a}{4} \equiv \frac{1}{a^4 g^2} \text{Tr} [\mathbb{1} - P_{ij}]. \quad (\text{B.4})$$

Once we couple the axion field and the gauge fields through the operator $\sim \kappa \varphi \epsilon_{ijk} F_{0i} F_{jk}$, we have freedom with the positioning of the objects appearing. In a “naive” discretization, we make use of \widehat{F}_{0i} from eq. (B.1) as a substitute for F_{0i} .²

²It has been argued that the topological charge density should be represented via an *improved* discretization. In the context of the Euclidean topological susceptibility, a symmetrized version of \widehat{F}_{0i} was introduced [54],

$$\langle \widehat{F}_{0i} \rangle(x) \equiv \frac{\widehat{F}_{0i}(x) + U_{-i}(x) \widehat{F}_{0i}(x - a\mathbf{i}) U_{-i}^\dagger(x)}{2}. \quad (\text{B.5})$$

Closer to our context, it was seen in ref. [23] that the real-time 2-point correlator of the improved topological charge density behaves more regularly at small time separations than that of the naive one. Our study differs from these previous contexts, as it involves a dynamical axion field, and 2-point correlators of the topological charge density do not appear directly. Nevertheless, we have also worked out the equations of motion following from eq. (B.5). In the end, we do *not* find any qualitative difference compared with the naive discretization. For instance, the time dependence of the Gauss constraint approximates to eq. (B.53) in both cases.

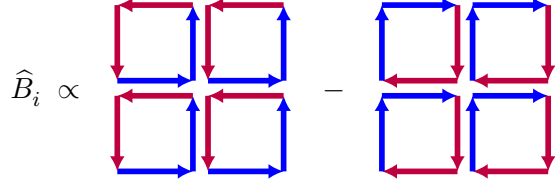


Figure 9: Illustration of the clover operator, defined in eq. (B.7). Red links are Hermitean conjugated, while the blue ones are not.

For the magnetic field, it is conventional to make use of a “clover” (cf. fig. 9),

$$\hat{B}_i(x) \equiv T^a \hat{B}_i^a(x), \quad \hat{B}_i^a(x) \equiv 2 \text{Tr} \left\{ T^a \left[\frac{\epsilon_{ijk} \langle \hat{F}_{jk} \rangle(x)}{2} \right] \right\}, \quad (\text{B.6})$$

$$\langle \hat{F}_{jk} \rangle(x) \equiv \frac{P_{jk} + P_{k-j} + P_{-j-k} + P_{-kj} - P_{kj} - P_{-jk} - P_{-k-j} - P_{j-k}}{8ia^2 g}. \quad (\text{B.7})$$

Here the movement in a negative direction is defined via $U_{-i}(x) \equiv U_i^\dagger(x - a\mathbf{i})$. In general the components of traceless matrices are obtained as

$$[\dots]^a \equiv 2 \text{Tr} \{ T^a [\dots] \}. \quad (\text{B.8})$$

With this notation, the lattice Lagrangian before gauge fixing can be written in a form analogous to eq. (A.3), *viz.*

$$\hat{L} \equiv a^3 \sum_{\mathbf{x}} \left\{ \frac{1}{2} \dot{\varphi}^2 - \frac{1}{2} \hat{\partial}_i \varphi \hat{\partial}_i \varphi - V(\varphi) + \frac{1}{2} \hat{F}_{0i}^a \hat{F}_{0i}^a - \frac{\widehat{F}_{ij}^a \widehat{F}_{ij}^a}{4} - \kappa \varphi \hat{F}_{0i}^a \hat{B}_i^a \right\}. \quad (\text{B.9})$$

The spatial derivative acting on φ , denoted by $\hat{\partial}_i$, can be defined as a difference.

While eq. (B.9) is a perfectly well-defined gauge-invariant Lagrangian, we have to be careful when we choose canonical coordinates. Naively a possibility could be to parametrize the links through gauge potentials via

$$U_i(x) \stackrel{?}{=} e^{iag A_i(x)}. \quad (\text{B.10})$$

One problem is that then derivatives become complicated,

$$(\partial_{A_i^a} U_i) U_i^\dagger = iag T^a + \frac{(iag)^2}{2} [A_i, T^a] + \frac{(iag)^3}{6} [A_i, [A_i, T^a]] + \dots, \quad (\text{B.11})$$

$$\dot{U}_i U_i^\dagger = iag \dot{A}_i + \frac{(iag)^2}{2} [A_i, \dot{A}_i] + \frac{(iag)^3}{6} [A_i, [A_i, \dot{A}_i]] + \dots. \quad (\text{B.12})$$

It is not clear how to re-express the right-hand sides in terms of the U_i in a useful way.

On the other hand, the right-hand side of eq. (B.12) is a traceless anti-Hermitean matrix. So we may define

$$\widehat{E}_i(x) \equiv \frac{1}{iag} [\dot{U}_i(x)] U_i^\dagger(x), \quad (\text{B.13})$$

implying

$$\dot{U}_i(x) = iag \widehat{E}_i(x) U_i(x), \quad \dot{U}_i^\dagger(x) = -iag U_i^\dagger(x) \widehat{E}_i(x). \quad (\text{B.14})$$

The challenge is to extract the corresponding coordinates \widehat{A}_i^a , needed for the Euler-Lagrange equations. Fortunately, we only need a derivative with respect to \widehat{A}_i^a , not the values of these coordinates themselves. The derivative can be defined via a left action on the group manifold (see, e.g., ref. [55]),

$$\frac{\partial f[U_i(x)]}{\partial \widehat{A}_i^a(x)} \equiv \nabla_{x,i}^a f[U_i(x)] \equiv \lim_{\epsilon \rightarrow 0} \frac{f[e^{iag\epsilon T^a} U_i(x)] - f[U_i(x)]}{\epsilon}. \quad (\text{B.15})$$

This guarantees that a time derivative can be expressed in a usual way,

$$\dot{f} = \sum_{\mathbf{x}, a, i} \widehat{E}_i^a(x) \nabla_{x,i}^a f. \quad (\text{B.16})$$

We adopt this implicit definition of the canonical coordinates in the following.

B.2. Gauss constraint and Hamiltonian

When we fix to the gauge $A_0^a = 0$, the Gauss constraint needs to be imposed as a consistency relation. Let us derive its discretized version. In analogy with eq. (A.5), it reads

$$0 = \widehat{G}(x) \equiv T^a \frac{\delta \widehat{L}}{\delta A_0^a(x)} \Big|_{A_0^a=0}, \quad (\text{B.17})$$

where we have defined $\delta \widehat{L}/\delta A_0^a \equiv (1/a^3) \partial \widehat{L}/\partial A_0^a$. We discuss separately the contributions present at $\kappa = 0$, and the corrections at first order in κ , writing

$$\widehat{G}(x) = \widehat{G}(x)|_{\kappa=0} + \widehat{G}(x)|_{\mathcal{O}(\kappa)}. \quad (\text{B.18})$$

At zeroth order, from eqs. (B.1) and (B.9), adopting the definition in eq. (B.13),

$$\widehat{G}(x)|_{\kappa=0} \stackrel{\substack{(\text{B.1}), (\text{B.9}) \\ (\text{B.13}), (\text{B.17})}}{=} \frac{1}{a} \sum_i [\widehat{E}_i(x) - U_{-i}(x) \widehat{E}_i(x - a\mathbf{i}) U_{-i}^\dagger(x)]. \quad (\text{B.19})$$

At first order,

$$\widehat{G}(x)|_{\mathcal{O}(\kappa)} \stackrel{\substack{(\text{B.1}), (\text{B.9}) \\ (\text{B.13}), (\text{B.17})}}{=} \frac{\kappa}{a} \sum_i [U_{-i}(x) \varphi(x - a\mathbf{i}) \widehat{B}_i(x - a\mathbf{i}) U_{-i}^\dagger(x) - \varphi(x) \widehat{B}_i(x)]. \quad (\text{B.20})$$

This generalizes the second term of eq. (A.5).

The Hamiltonian is obtained from a Legendre transform like in eq. (A.7). By construction, terms depending linearly on \hat{E}_i^a cancel in the Legendre transform, which then leads to

$$\hat{H} \stackrel{(B.9)}{=} \stackrel{(A.7)}{=} a^3 \sum_{\mathbf{x}} \left\{ \frac{1}{2} \dot{\varphi}^2 + \frac{1}{2} \hat{\partial}_i \varphi \hat{\partial}_i \varphi + V(\varphi) + \frac{1}{2} \hat{E}_i^a \hat{E}_i^a + \frac{1}{a^4 g^2} \sum_{i,j} \text{Tr} [\mathbb{1} - P_{ij}] \right\}. \quad (B.21)$$

B.3. Evolution equations

The Euler-Lagrange equations are obtained like in eq. (A.9). On the left-hand side,

$$\frac{\delta \hat{L}}{\delta \hat{E}_i^a(x)} \bigg|_{A_0^a=0} \stackrel{(B.9)}{=} \stackrel{(B.15)}{=} \hat{E}_i^a(x) - \kappa \varphi(x) \hat{B}_i^a(x). \quad (B.22)$$

In order to work out the right-hand side, we introduce the short-hand notation

$$Q_{mn\dots}(y) f \equiv U_m(y) U_n(y + a\mathbf{m}) \dots f(y + am\mathbf{m} + an\mathbf{n} + \dots), \quad (B.23)$$

which implies $U_i = Q_i$ and $P_{ij} = Q_{ij-i-j}$. Then, for a single plaquette, eq. (B.15) yields

$$\begin{aligned} \frac{\partial P_{jk}(y)}{\partial \hat{A}_i^a(x)} &\stackrel{(B.3)}{=} \stackrel{(B.15)}{=} i \text{ag} \left\{ \delta_{i,j} \left[\delta_{\mathbf{x},\mathbf{y}} T^a Q_{jk-j-k}(x) - \delta_{\mathbf{x},\mathbf{y}+a\mathbf{k}} Q_{jk-j}(y) T^a Q_{-k}(x) \right] \right. \\ &\quad \left. + \delta_{i,k} \left[\delta_{\mathbf{x},\mathbf{y}+a\mathbf{j}} Q_j(y) T^a Q_{k-j-k}(x) - \delta_{\mathbf{x},\mathbf{y}} Q_{jk-j-k}(x) T^a \right] \right\}. \end{aligned} \quad (B.24)$$

After taking a trace, this leads to the first line of eq. (B.33).

In contrast, the terms of $\mathcal{O}(\kappa)$ are cumbersome. Moving the second term from eq. (B.22) on the right-hand side, we get

$$\dot{\hat{E}}_i^a(x) \bigg|_{\mathcal{O}(\kappa)} \stackrel{(A.9)}{=} \stackrel{(B.9),(B.22)}{=} \kappa \left\{ \dot{\varphi}(x) \hat{B}_i^a(x) + \varphi(x) \dot{\hat{B}}_i^a(x) - \sum_{\mathbf{y},c,j} \hat{E}_j^c(y) \varphi(y) \nabla_{x,i}^a \hat{B}_j^c(y) \right\}. \quad (B.25)$$

The time derivative of the magnetic field on the second line of eq. (B.25) can be taken with eq. (B.16). After some algebra we obtain, employing the notation from eq. (B.8),

$$\dot{\hat{B}}_i^a(x) = \frac{\epsilon_{ijk} \{\Phi_{jk}(x)\}^a}{8a}, \quad (B.26)$$

where, making use of the notation in eq. (B.23),

$$\begin{aligned} \Phi_{jk} &= \hat{E}_j Q_{jk-j-k} + \hat{E}_k Q_{k-j-kj} - Q_{-kjk-j} \hat{E}_j - Q_{jk-j-k} \hat{E}_k \\ &\quad + Q_{-k} \hat{E}_j Q_{jk-j} + Q_j \hat{E}_k Q_{k-j-k} - Q_{-j} \hat{E}_j Q_{-kjk} - Q_{-k} \hat{E}_k Q_{jk-j} \\ &\quad + Q_{-j-k} \hat{E}_j Q_{jk} + Q_{-kj} \hat{E}_k Q_{k-j} - Q_{k-j} \hat{E}_j Q_{-kj} - Q_{-j-k} \hat{E}_k Q_{jk} \\ &\quad + Q_{k-j-k} \hat{E}_j Q_j + Q_{-j-kj} \hat{E}_k Q_k - Q_{jk-j} \hat{E}_j Q_{-k} - Q_{k-j-k} \hat{E}_k Q_j. \end{aligned} \quad (B.27)$$

From the last term of eq. (B.25), we get

$$-\sum_{\mathbf{y},c,j} \widehat{E}_j^c(y) \varphi(y) \nabla_{x,i}^a \widehat{E}_j^c(y) = \frac{\epsilon_{ijk} \{\Theta_{ijk}(x)\}^a}{8a}, \quad (\text{B.28})$$

where

$$\begin{aligned} \Theta_{ijk} = & \varphi \widehat{E}_j Q_{ki-k-i} - \varphi \widehat{E}_j Q_{-kik-i} + Q_{ik-i-k} \varphi \widehat{E}_j - Q_{i-k-ik} \varphi \widehat{E}_j \\ & + Q_k \varphi \widehat{E}_j Q_{i-k-i} + Q_i \varphi \widehat{E}_j Q_{k-i-k} - Q_{-k} \varphi \widehat{E}_j Q_{ik-i} - Q_i \varphi \widehat{E}_j Q_{-k-ik} \\ & + Q_{ki} \varphi \widehat{E}_j Q_{-k-i} + Q_{ik} \varphi \widehat{E}_j Q_{-i-k} - Q_{-ki} \varphi \widehat{E}_j Q_{k-i} - Q_{i-k} \varphi \widehat{E}_j Q_{-ik} \\ & + Q_{ki-k} \varphi \widehat{E}_j Q_{-i} + Q_{ik-i} \varphi \widehat{E}_j Q_{-k} - Q_{i-k-i} \varphi \widehat{E}_j Q_k - Q_{-kik} \varphi \widehat{E}_j Q_{-i}. \end{aligned} \quad (\text{B.29})$$

In a practical implementation, it is important to minimize matrix multiplications. In particular, eq. (B.29) can be regrouped in various ways for this purpose, for instance

$$\begin{aligned} \Theta_{ijk} \stackrel{(\text{B.29})}{=} & (\varphi \widehat{E}_j Q_{ki} + Q_k \varphi \widehat{E}_j Q_i + Q_{ki} \varphi \widehat{E}_j) Q_{-k-i} \\ & - (\varphi \widehat{E}_j Q_{-ki} + Q_{-k} \varphi \widehat{E}_j Q_i + Q_{-ki} \varphi \widehat{E}_j) Q_{k-i} \\ & + Q_i \varphi \widehat{E}_j (Q_{k-i-k} - Q_{-k-ik}) + \text{H.c.}, \end{aligned} \quad (\text{B.30})$$

where “H.c.” denotes Hermitean conjugation of the whole expression.

Putting everything together, the analogues of eqs. (A.14)–(A.16) can be expressed as

$$\ddot{\varphi}(x) = \widehat{\Delta} \varphi(x) - V'(\varphi) - \kappa \sum_{a,i} \widehat{E}_i^a(x) \widehat{B}_i^a(x), \quad (\text{B.31})$$

$$\dot{U}_i(x) = i a g \widehat{E}_i(x) U_i(x), \quad (\text{B.32})$$

$$\begin{aligned} \dot{\widehat{E}}_i^a(x) = & \frac{i}{a^3 g} \sum_j \text{Tr} \{ T^a [P_{ij} + P_{i-j} - P_{ji} - P_{-ji}] (x) \} \\ & + \kappa \left\{ \dot{\varphi}(x) \widehat{B}_i(x) + \sum_{j,k} \frac{\epsilon_{ijk} [\varphi(x) \Phi_{jk}(x) + \Theta_{ijk}(x)]}{8a} \right\}^a, \end{aligned} \quad (\text{B.33})$$

where $\widehat{\Delta}$ is a lattice Laplacian. In comparison with eq. (A.16), the first row of eq. (B.33) represents $-\mathcal{D} \times \mathbf{B}$, the terms on the second row $\kappa \dot{\varphi} \mathbf{B}$ and $-\kappa \nabla \varphi \times \mathbf{E}$, respectively.

Even though eqs. (B.31)–(B.33) constitute the perfect analogue of the continuum equations in eqs. (A.14)–(A.16), we find it efficient to reorganize them. Specifically, let us define

$$\widehat{\Pi}_i^a(x) \equiv \widehat{E}_i^a(x) - \kappa \varphi(x) \widehat{B}_i^a(x). \quad (\text{B.34})$$

It follows from eqs. (B.25) and (B.26) that if we compute the time evolution of $\widehat{\Pi}_i^a$, then the complicated object Φ_{jk} , given in eq. (B.27), does not need to be evaluated.

Furthermore, we rescale variables and parameters into dimensionless forms. For this we make use of the physical length scale, ℓ , introduced in eq. (2.20). In principle it could be associated for instance with the inverse Hubble rate during inflation, H^{-1} , or the inverse mass, m^{-1} . In the absence of expansion, we follow the latter possibility (cf. eq. (2.20)). All dimensionful quantities (fields, coordinates, parameters) are scaled with ℓ so as to make them dimensionless,

$$\tilde{\varphi} \equiv \ell \varphi, \quad \tilde{E}_i^a \equiv \ell^2 \hat{E}_i^a, \quad \tilde{B}_i^a \equiv \ell^2 \hat{B}_i^a, \quad \tilde{\Theta}_{ijk}^a \equiv \ell^3 \Theta_{ijk}^a, \quad (\text{B.35})$$

$$\tilde{t} \equiv t/\ell, \quad \tilde{a} \equiv a/\ell, \quad \tilde{k} \equiv \ell k, \quad \tilde{\omega}_k \equiv \ell \omega_k, \quad (\text{B.36})$$

$$\tilde{\kappa} \equiv \kappa/\ell, \quad \tilde{m} \equiv \ell m. \quad (\text{B.37})$$

The gauge coupling, g^2 , is dimensionless and does not get scaled in the classical theory (it should be thought of as a renormalized coupling, $g^2(\bar{\mu} \sim 1/\ell)$).

Being also explicit about the lattice Laplacian, and inserting the potential from eq. (2.10), it follows from eqs. (B.31)–(B.37) that

$$\partial_t^2 \tilde{\varphi}(x) = \sum_i \frac{\tilde{\varphi}(x + a\mathbf{i}) - 2\tilde{\varphi}(x) + \tilde{\varphi}(x - a\mathbf{i})}{\tilde{a}^2} - \tilde{m}^2 \tilde{\varphi} - \tilde{\kappa} \sum_{a,i} \tilde{E}_i^a(x) \overbrace{\tilde{B}_i^a(x)}^{(\text{B.6})}, \quad (\text{B.38})$$

$$\partial_t U_i(x) = i\tilde{a}g \tilde{E}_i(x) U_i(x), \quad (\text{B.39})$$

$$\partial_t \tilde{\Pi}_i^a(x) \stackrel{\substack{(\text{B.33}) \\ (\text{B.26})}}{=} \sum_j \frac{i \text{Tr} \{ T^a [P_{ij} + P_{i-j} - P_{ji} - P_{-ji}](x) \}}{\tilde{a}^3 g} + \sum_{j,k} \frac{\tilde{\kappa} \epsilon_{ijk} \overbrace{\tilde{\Theta}_{ijk}^a(x)}^{(\text{B.30})}}{8\tilde{a}}, \quad (\text{B.40})$$

$$\tilde{E}_i^a \stackrel{(\text{B.34})}{=} \tilde{\Pi}_i^a + \tilde{\kappa} \tilde{\varphi} \tilde{B}_i^a. \quad (\text{B.41})$$

What this means is that we evolve the scalar field with eq. (B.38), the links with eq. (B.39), and $\tilde{\Pi}_i^a$ with eq. (B.40). For the next time step, we solve for \tilde{E}_i^a from eq. (B.41).

As an example of a physical quantity, we note from eq. (B.21) that the energy density associated with the electric fields is $e \equiv E/V \supset \frac{1}{2} \hat{E}_i^a \hat{E}_i^a$. In units of ℓ , this becomes $\ell^4 e \supset \frac{1}{2} \tilde{E}_i^a \tilde{E}_i^a$. When we represent this in terms of a power spectrum (cf. sec. B.6), the ultraviolet (Rayleigh-Jeans) problem of classical field theory lies in the fact that in the course of time, much of the energy density transitions to momenta $k \sim 1/a$, i.e. $\tilde{k} \sim 1/\tilde{a} \gg 1$ (cf. sec. 5.3).

B.4. Energy conservation

Consider the time derivative of the Hamiltonian from eq. (B.21),

$$\dot{\hat{H}} \stackrel{(B.21)}{=} a^3 \sum_{\mathbf{x}} \left\{ \dot{\varphi} \ddot{\varphi} - \dot{\varphi} \hat{\Delta} \varphi + \dot{\varphi} V'(\varphi) + \hat{E}_i^a \dot{\hat{E}}_i^a - \frac{1}{a^4 g^2} \sum_{i,j} \text{Tr} [\dot{P}_{ij}] \right\}. \quad (B.42)$$

At order $\kappa = 0$, the scalar field parts cancel directly thanks to eq. (B.31). For the electric field part at $\kappa = 0$, the first row of eq. (B.33) yields

$$\dot{\hat{H}}|_{\kappa=0} \stackrel{(B.42)}{\supset} \frac{i}{g} \sum_{\mathbf{x}, i, j} \text{Tr} \{ \hat{E}_i(x) [P_{ij} + P_{i-j} - P_{ji} - P_{-ji}] (x) \}. \quad (B.43)$$

From the plaquette in the last term of eq. (B.42), we obtain

$$\dot{\hat{H}}|_{\kappa=0} \stackrel{(B.16)}{\supset} \stackrel{(B.24)}{\supset} -\frac{i}{g} \sum_{\mathbf{x}, i, j} \text{Tr} \{ \hat{E}_i(x) P_{ij}(x) - P_{-ji}(x) \hat{E}_i(x) + \hat{E}_i(x) P_{i-j}(x) - P_{ji}(x) \hat{E}_i(x) \}. \quad (B.44)$$

Using the cyclic property of the trace, eqs. (B.43) and (B.44) cancel against each other.

Proceeding to $\mathcal{O}(\kappa)$, the last term of eq. (B.31) and the second term of eq. (B.33) yield

$$\dot{\hat{H}}|_{\mathcal{O}(\kappa)} \stackrel{(B.42)}{\supset} \stackrel{(B.31), (B.33)}{\supset} \kappa a^3 \sum_{\mathbf{x}, c, i} \left\{ -\dot{\varphi}(x) \hat{E}_i^c(x) \hat{B}_i^c(x) + \hat{E}_i^c(x) \dot{\varphi}(x) \hat{B}_i^c(x) \right\}, \quad (B.45)$$

which clearly cancel. Finally, for the contributions originating from the third term of eq. (B.33), the terms from Φ_{jk} and Θ_{ijk} both give structures containing two electric fields, connected by Q 's. Shifting \mathbf{x} , re-ordering terms inside the trace, and renaming indices, all 16 terms find a counterpart on the other side, and cancel exactly.

B.5. Time dependence of the Gauss constraint

Turning to the Gauss constraint from eq. (B.18), the goal is to see whether it is time-independent. Let us first inspect its $\kappa = 0$ part, given by eq. (B.19). We note that two of the terms from $\dot{\hat{G}}$ immediately cancel as a consequence of eq. (B.32),

$$-\underbrace{\dot{U}_i^\dagger(x - a\mathbf{i})}_{-iagU_i^\dagger(x - a\mathbf{i})} \hat{E}_i(x - a\mathbf{i}) U_i(x - a\mathbf{i}) - U_i^\dagger(x - a\mathbf{i}) \hat{E}_i(x - a\mathbf{i}) \underbrace{\dot{U}_i(x - a\mathbf{i})}_{+iag\hat{E}_i(x - a\mathbf{i})U_i(x - a\mathbf{i})} = 0. \quad (B.46)$$

Therefore

$$\dot{\hat{G}}(x)|_{\kappa=0} \stackrel{(B.19)}{=} \frac{1}{a} \sum_i \left[\dot{\hat{E}}_i(x)|_{\kappa=0} - U_{-i}(x) \dot{\hat{E}}_i(x - a\mathbf{i})|_{\kappa=0} U_{-i}^\dagger(x) \right]. \quad (B.47)$$

The time derivatives are given by the first row of eq. (B.33). When we sum over the generators T^a to obtain $\dot{\hat{E}}_i = T^a \dot{\hat{E}}_i^a$, then the result has the form

$$\sum_a T_{mn}^a \text{Tr} \{ T^a M \} = \underbrace{\sum_a T_{mn}^a T_{kl}^a M_{lk}}_{\frac{1}{2} (\delta_{ml} \delta_{nk} - \frac{1}{N_c} \delta_{mn} \delta_{kl})} = \frac{1}{2} \left(M_{mn} - \frac{\delta_{mn} \text{Tr} M}{N_c} \right). \quad (\text{B.48})$$

It is enough to consider the first term, as the second term just subtracts its trace part, which vanishes if the term itself vanishes. Then the second term in eq. (B.47) re-orders the indices of the plaquettes, and we get

$$\dot{\hat{G}}(x) \Big|_{\kappa=0} \stackrel{\text{(B.33)}}{\supseteq} \stackrel{\text{(B.47)}}{\supseteq} \frac{i}{2a^4 g} \sum_{ij} \{ P_{ij} + P_{i-j} - P_{ji} - P_{-ji} - P_{j-i} - P_{-j-i} + P_{-ij} + P_{-i-j} \}. \quad (\text{B.49})$$

The summand is antisymmetric in $i \leftrightarrow j$, and therefore the sum vanishes.

Proceeding to the part of $\mathcal{O}(\kappa)$, eqs. (B.19) and (B.20) yield

$$\begin{aligned} \dot{\hat{G}}(x) \Big|_{\mathcal{O}(\kappa)} &\stackrel{\text{(B.19)}}{=} \stackrel{\text{(B.20)}}{=} \frac{1}{a} \sum_i \left\{ \dot{\hat{E}}_i(x) \Big|_{\mathcal{O}(\kappa)} - U_{-i}(x) \dot{\hat{E}}_i(x - a\mathbf{i}) \Big|_{\mathcal{O}(\kappa)} U_{-i}^\dagger(x) \right\} \\ &+ \frac{\kappa}{a} \sum_i \left\{ \dot{\varphi}(x - a\mathbf{i}) U_{-i}(x) \hat{B}_i(x - a\mathbf{i}) U_{-i}^\dagger(x) - \dot{\varphi}(x) \hat{B}_i(x) \right. \\ &\quad \left. + \varphi(x - a\mathbf{i}) \partial_t [U_{-i}(x) \hat{B}_i(x - a\mathbf{i}) U_{-i}^\dagger(x)] - \varphi(x) \dot{\hat{B}}_i(x) \right\}. \end{aligned} \quad (\text{B.50})$$

Inserting the second term of eq. (B.33) for the first row of eq. (B.50), the resulting terms cancel against the second row of eq. (B.50).

It remains to combine the third term of eq. (B.33) with the third row of eq. (B.50). The terms containing Φ_{jk} cancel exactly against the time derivatives of \hat{B}_i from the third row of eq. (B.50). For the terms containing Θ_{ijk} , we find an almost complete cancellation after renaming indices and making use of antisymmetry, leaving over just

$$\begin{aligned} \dot{\hat{G}}(x) \Big|_{\mathcal{O}(\kappa)} &\supseteq \frac{\kappa}{8a^2} \sum_{i,j,k} \epsilon_{ijk} \{ \Theta_{ijk}(x) - U_{-i}(x) \Theta_{ijk}(x - a\mathbf{i}) U_{-i}^\dagger(x) \} \\ &= \frac{\kappa}{8a^2} \sum_{i,j,k} \epsilon_{ijk} [\varphi \hat{E}_i, P_{jk} + P_{k-j} + P_{-j-k} + P_{-k-j}]. \end{aligned} \quad (\text{B.51})$$

Commutators similar to eq. (B.51) arise also from when ∂_t acts on U_i or U_i^\dagger on the third row of eq. (B.50). Combining the latter terms with eq. (B.51), and re-expressing the result in terms of the magnetic field from eqs. (B.6) and (B.7), we find the full result

$$\begin{aligned} \dot{\hat{G}}(x) &= ig\kappa \sum_i \left\{ \varphi(x) [\hat{E}_i(x), \hat{B}_i(x)] \right. \\ &\quad \left. - U_{-i}(x) \varphi(x - a\mathbf{i}) [\hat{E}_i(x - a\mathbf{i}), \hat{B}_i(x - a\mathbf{i})] U_{-i}^\dagger(x) \right\}. \end{aligned} \quad (\text{B.52})$$

In general, eq. (B.52) is non-vanishing. However, because it contains commutators, it vanishes in an Abelian theory, and because it is composed of a difference of two similar terms, it vanishes when the lattice spacing a is small compared with the dynamical scales of the system ($a \ll \ell$). To be specific about the latter, a formal expansion in a gives

$$\dot{\tilde{G}}(x) \simeq ig\kappa \sum_i \{ a [D_i, \varphi(x) [E_i(x), B_i(x)]] + \mathcal{O}(a^2) \}. \quad (\text{B.53})$$

For the lattice spacing that we have used in practice (cf. eq. (4.1)), this time evolution is numerically slow, but nevertheless clearly observable in the SU(2) case.

It is unclear to us whether the existence of eq. (B.53) has a deeper reason, related to the non-topological nature of the lattice discretization of the topological charge density. From the simulation point of view, it however represents no practical challenge.

B.6. Initial conditions and power spectra

When we study the system on a lattice, the initial conditions in eqs. (2.12)–(2.15) need to be rewritten. With a finite lattice spacing, a , and a finite lattice extent, N , across which period boundary conditions are imposed, momenta, integrals, and δ -constraints take the forms

$$\mathbf{k} \rightarrow \mathbf{k}(\mathbf{n}) \equiv \frac{2\pi\mathbf{n}}{aN}, \quad \mathbf{n} \in \left[-\frac{N}{2}, \dots, \frac{N}{2} - 1 \right]^3, \quad (\text{B.54})$$

$$\int_{\mathbf{k}} \xrightarrow[\text{(B.54)}]{\text{(A.19)}} \frac{1}{a^3 N^3} \sum_{\mathbf{n}}, \quad \langle c_{\mathbf{n}} c_{\mathbf{m}}^* \rangle \xrightarrow{\text{(2.14)}} f_k a^3 N^3 \delta_{\mathbf{n}, \mathbf{m} \text{ mod } \mathbf{N}}. \quad (\text{B.55})$$

It is convenient to normalize the noise close to unity, so we rescale $c_{\mathbf{n}} \rightarrow \sqrt{a^3 N^3} \hat{c}_{\mathbf{n}}$. Furthermore, we rescale fields and momenta according to eqs. (B.35) and (B.36), respectively. Then eqs. (2.12) and (2.13) become

$$\tilde{\varphi}(0, \mathbf{x}) = \frac{1}{\sqrt{\tilde{a}^3 N^3}} \sum_{\mathbf{n}} [\hat{c}_{\mathbf{n}} \tilde{\varphi}_k(0) e^{i\mathbf{k}(\mathbf{n}) \cdot \mathbf{x}} + \hat{c}_{\mathbf{n}}^* \tilde{\varphi}_k^*(0) e^{-i\mathbf{k}(\mathbf{n}) \cdot \mathbf{x}}], \quad (\text{B.56})$$

$$\partial_{\tilde{t}} \tilde{\varphi}(0, \mathbf{x}) = \frac{1}{\sqrt{\tilde{a}^3 N^3}} \sum_{\mathbf{n}} (i\tilde{\omega}_k) [-\hat{c}_{\mathbf{n}} \tilde{\varphi}_k(0) e^{i\mathbf{k}(\mathbf{n}) \cdot \mathbf{x}} + \hat{c}_{\mathbf{n}}^* \tilde{\varphi}_k^*(0) e^{-i\mathbf{k}(\mathbf{n}) \cdot \mathbf{x}}], \quad (\text{B.57})$$

where $\tilde{k} \equiv |\tilde{\mathbf{k}}(\mathbf{n})|$ according to eqs. (B.36) and (B.54); $\tilde{\varphi}_k(0) \equiv 1/\sqrt{2\tilde{\omega}_k}$ according to eqs. (A.20) and (B.36); and $\langle \hat{c}_{\mathbf{n}} \hat{c}_{\mathbf{m}}^* \rangle = f_k \delta_{\mathbf{n}, \mathbf{m}}$, where f_k is from eq. (2.15).

It is appropriate to stress that the mode function, $\tilde{\varphi}_k$, involves the energy of the corresponding mode, $\tilde{\omega}_k$ (cf. eq. (A.20)). On the lattice, because of the discretized Lagrangian in eq. (B.38), the kinetic energy gets modified, becoming a trigonometric function. However, we insert noise only in the IR domain $\tilde{k} \leq 50 \ll 2\pi/\tilde{a}$ (cf. eq. (4.1)), where the dispersion relation is to a reasonable approximation continuum-like.

Power spectra at finite times are obtained from spatial Fourier transforms, like in eqs. (2.17) and (2.18). On the lattice, and in rescaled units, the Fourier transform becomes

$$G_{\tilde{\varphi}}(t, \mathbf{k}) \stackrel{(2.17)}{=} \stackrel{(B.54)}{\tilde{a}^3} \sum_{\mathbf{x}} e^{-i\frac{2\pi\mathbf{n}}{N} \cdot \frac{\mathbf{x}}{a}} \langle \tilde{\varphi}(t, \mathbf{x}) \tilde{\varphi}(t, \mathbf{0}) \rangle, \quad \frac{\mathbf{x}}{a} \in [0, 1, \dots, N-1]^3 \quad (B.58)$$

$$= \frac{1}{\tilde{a}^3 N^3} \langle |\tilde{\varphi}(t, \mathbf{k})|^2 \rangle = \frac{\tilde{a}^3}{N^3} \left\langle \left| \sum_{\mathbf{x}} e^{-i\frac{2\pi\mathbf{n}}{N} \cdot \frac{\mathbf{x}}{a}} \tilde{\varphi}(t, \mathbf{x}) \right|^2 \right\rangle. \quad (B.59)$$

Continuous rotational symmetry is absent, but at small $\tilde{k} \ll 2\pi/\tilde{a}$ we can nevertheless define a power spectrum like in eq. (2.18),

$$\mathcal{P}_{\tilde{\varphi}}(t, \tilde{k}) \equiv \frac{\tilde{k}^3 G_{\tilde{\varphi}}(t, \mathbf{k})}{2\pi^2}. \quad (B.60)$$

It is useful to carry out a consistency check on the conventions adopted. If we take the initial condition from eq. (B.56), then

$$\langle \tilde{\varphi}(0, \mathbf{x}) \tilde{\varphi}(0, \mathbf{0}) \rangle \stackrel{(B.56)}{=} \frac{1}{\tilde{a}^3 N^3} \sum_{\mathbf{n}} |\tilde{\varphi}_k(0)|^2 f_k [e^{i\mathbf{k}(\mathbf{n}) \cdot \mathbf{x}} + e^{-i\mathbf{k}(\mathbf{n}) \cdot \mathbf{x}}]. \quad (B.61)$$

The Fourier transform then becomes (denoting its argument now by \mathbf{q} , and re-ordering sums)

$$\begin{aligned} G_{\tilde{\varphi}}(0, \mathbf{q}) &\stackrel{(B.58)}{=} \stackrel{(B.61)}{\frac{1}{N^3}} \sum_{\mathbf{n}} |\tilde{\varphi}_k(0)|^2 f_k \sum_{\mathbf{x}} [e^{i(\mathbf{k}(\mathbf{n}) - \mathbf{q}) \cdot \mathbf{x}} + e^{-i(\mathbf{k}(\mathbf{n}) + \mathbf{q}) \cdot \mathbf{x}}] \\ &= \sum_{\mathbf{n}} |\tilde{\varphi}_k(0)|^2 f_k \left[\delta_{\mathbf{k}(\mathbf{n}), \mathbf{q}} + \delta_{\mathbf{k}(\mathbf{n}), -\mathbf{q}} \right] \\ &= 2|\tilde{\varphi}_q(0)|^2 f_q. \end{aligned} \quad (B.62)$$

Multiplying with the factor from eq. (B.60), and inserting f_q from eq. (2.14), then reproduces the power spectrum in eq. (A.22) for small momenta, $q < \Lambda$.

Proceeding to the initial condition for the electric field, we follow ref. [56] and adopt a discretized version of eq. (A.24). The spatial links are set to unity in the initial state, corresponding to the vanishing of the magnetic field. The Gauss constraint from eq. (B.20) then drops out. In order to satisfy eq. (B.19), the polarization vectors need to fulfill

$$0 \stackrel{(B.19)}{=} \sum_i (\mathbf{e}_{\mathbf{k}}^{\lambda})_i \frac{2}{\tilde{a}} \sin\left(\frac{\tilde{a}\tilde{k}_i}{2}\right) \stackrel{\tilde{a} \ll 1}{\approx} \sum_i (\mathbf{e}_{\mathbf{k}}^{\lambda})_i \tilde{k}_i. \quad (B.63)$$

Starting with an ansatz, for instance $\mathbf{e}_{\mathbf{k}}^0 \equiv (1, 1, \sqrt{2})^T/2$, and denoting $\mathbf{v} \equiv \tilde{\mathbf{k}}/\tilde{k}$, two (linear) polarization states can be constructed as $\mathbf{e}_{\mathbf{k}}^1 = \mathcal{N} [\mathbf{e}_{\mathbf{k}}^0 - (\mathbf{e}_{\mathbf{k}}^0 \cdot \mathbf{v}) \mathbf{v}]$ and $\mathbf{e}_{\mathbf{k}}^2 = \mathbf{v} \times \mathbf{e}_{\mathbf{k}}^1$, where \mathcal{N} is a normalization factor. Given that the components of $\tilde{\mathbf{k}}$ are rational (modulo π ; cf. eq. (B.54)), the irrational $\sqrt{2}$ in $\mathbf{e}_{\mathbf{k}}^0$ guarantees that $\mathbf{e}_{\mathbf{k}}^1 \neq \mathbf{0} \neq \mathbf{e}_{\mathbf{k}}^2$ for all \mathbf{k} .

References

- [1] N. Aghanim *et al* [Planck], *Planck 2018 results. VI. Cosmological parameters*, Astron. Astrophys. 641 (2020) A6; *ibid.* 652 (2021) C4 (erratum) [1807.06209].
- [2] T. Louis *et al.*, *The Atacama Cosmology Telescope: DR6 Power Spectra, Likelihoods and Λ CDM Parameters*, JCAP 11 (2025) 062 [2503.14452].
- [3] J.A. Zebrowski *et al.* [SPT-3G], *Constraints on Inflationary Gravitational Waves with Two Years of SPT-3G Data*, Phys. Rev. D 112 (2025) 123520 [2505.02827].
- [4] K. Freese, J.A. Frieman and A.V. Olinto, *Natural inflation with pseudo Nambu-Goldstone bosons*, Phys. Rev. Lett. 65 (1990) 3233.
- [5] R.D. Peccei and H.R. Quinn, *CP Conservation in the Presence of Pseudoparticles*, Phys. Rev. Lett. 38 (1977) 1440.
- [6] S. Weinberg, *A New Light Boson?*, Phys. Rev. Lett. 40 (1978) 223.
- [7] F. Wilczek, *Problem of Strong P and T Invariance in the Presence of Instantons*, Phys. Rev. Lett. 40 (1978) 279.
- [8] F. Takahashi and W. Yin, *Challenges for heavy QCD axion inflation*, JCAP 10 (2021) 057 [2105.10493].
- [9] M.M. Anber and L. Sorbo, *Naturally inflating on steep potentials through electromagnetic dissipation*, Phys. Rev. D 81 (2010) 043534 [0908.4089].
- [10] M.M. Anber and L. Sorbo, *Non-Gaussianities and chiral gravitational waves in natural steep inflation*, Phys. Rev. D 85 (2012) 123537 [1203.5849].
- [11] D.G. Figueroa *et al.*, *Nonlinear dynamics of axion inflation: A detailed lattice study*, Phys. Rev. D 111 (2025) 063545 [2411.16368].
- [12] O. Iarygina, E.I. Sfakianakis and A. Brandenburg, *Schwinger effect in axion inflation on a lattice*, [2506.20538].
- [13] D. Jamieson, A. Caravano and E. Komatsu, *Primordial power spectrum and bispectrum from lattice simulations of axion-U(1) inflation*, Phys. Rev. D 112 (2025) 103531 [2507.22285].
- [14] R. von Eckardstein, *GEFF: The Gradient Expansion Formalism Factory — A tool for inflationary gauge-field production*, [2510.12644].
- [15] Y. Fu, J. Ghiglieri, S. Iqbal and A. Kurkela, *Thermalization of non-Abelian gauge theories at next-to-leading order*, Phys. Rev. D 105 (2022) 054031 [2110.01540].
- [16] W. DeRocco, P.W. Graham and S. Kalia, *Warming up cold inflation*, JCAP 11 (2021) 011 [2107.07517].
- [17] T. Fujita, K. Mukaida and T. Tsuji, *Reheating after axion inflation*, JCAP 07 (2025) 002 [2503.01228].
- [18] E. Broadberry, A. Hook and S. Mondal, *Warm Inflation with Pseudo-scalar couplings*, [2505.07943].

- [19] S. Bhattacharya, M. Fasiello, A. Papageorgiou and E. Dimastrogiovanni, *On the prospects of thermalization of axion-SU(2) inflation*, JCAP 10 (2025) 080 [2506.11853].
- [20] L. McLerran, E. Mottola and M.E. Shaposhnikov, *Sphalerons and axion dynamics in high-temperature QCD*, Phys. Rev. D 43 (1991) 2027.
- [21] M. Laine and S. Procacci, *Minimal warm inflation with complete medium response*, JCAP 06 (2021) 031 [2102.09913].
- [22] G.D. Moore and M. Tassler, *The sphaleron rate in SU(N) gauge theory*, JHEP 02 (2011) 105 [1011.1167].
- [23] M. Laine, L. Niemi, S. Procacci and K. Rummukainen, *Shape of the hot topological charge density spectral function*, JHEP 11 (2022) 126 [2209.13804].
- [24] K.V. Berghaus, P.W. Graham and D.E. Kaplan, *Minimal warm inflation*, JCAP 03 (2020) 034; *ibid.* 10 (2023) E02 (erratum) [1910.07525].
- [25] J. Yokoyama and A.D. Linde, *Is warm inflation possible?*, Phys. Rev. D 60 (1999) 083509 [hep-ph/9809409].
- [26] M. Mirbabayi and A. Gruzinov, *Shapes of non-Gaussianity in warm inflation*, JCAP 02 (2023) 012 [2205.13227].
- [27] G. Ballesteros, A. Pérez Rodríguez and M. Pierre, *Monomial warm inflation revisited*, JCAP 03 (2024) 003 [2304.05978].
- [28] G. Montefalcone, V. Aragam, L. Visinelli and K. Freese, *WarmSPy: a numerical study of cosmological perturbations in warm inflation*, JCAP 01 (2024) 032 [2306.16190].
- [29] G.S. Rodrigues and R.O. Ramos, *WI2easy: warm inflation dynamics made easy*, JCAP 09 (2025) 014 [2504.17760].
- [30] M. Laine, S. Procacci and A. Rogelj, *Evolution of coupled scalar perturbations through smooth reheating. II. Thermal fluctuation regime*, JCAP 12 (2025) 058 [2507.12849].
- [31] K.V. Berghaus, M. Drewes and S. Zell, *Warm Inflation with the Standard Model*, Phys. Rev. Lett. 135, 2025 171002 [2503.18829].
- [32] R.O. Ramos and G.S. Rodrigues, *Viability of warm inflation with standard model interactions*, Phys. Rev. D 111 (2025) 123527 [2504.20943].
- [33] M. Bastero-Gil, A. Berera, I. G. Moss and R. O. Ramos, *Theory of non-Gaussianity in warm inflation*, JCAP 12 2014 008 [1408.4391].
- [34] M. Mirbabayi, *Loosely coupled particles in warm inflation*, JCAP 05 (2025) 067 [2409.17927].
- [35] Y. Qiu and L. Sorbo, *Spectrum of tensor perturbations in warm inflation*, Phys. Rev. D 104 (2021) 083542 [2107.09754].
- [36] P. Klose, M. Laine and S. Procacci, *Gravitational wave background from non-Abelian reheating after axion-like inflation*, JCAP 05 (2022) 021 [2201.02317].

[37] P. Klose, M. Laine and S. Procacci, *Gravitational wave background from vacuum and thermal fluctuations during axion-like inflation*, JCAP 12 (2022) 020 [2210.11710].

[38] G. Montefalcone, B. Shams Es Haghi, T. Xu and K. Freese, *Thermal gravitons from warm inflation*, Phys. Rev. D 112 (2025) 063556 [2507.08739].

[39] Q. Chen *et al.*, *Freeze-in gravitational waves and dark matter in warm inflation*, [2507.13916].

[40] H. Kolesova, M. Laine and S. Procacci, *Maximal temperature of strongly-coupled dark sectors*, JHEP 05 (2023) 239 [2303.17973].

[41] V. Domcke and S. Sandner, *The Different Regimes of Axion Gauge Field Inflation*, JCAP 09 (2019) 038 [1905.11372].

[42] O. Iarygina, E.I. Sfakianakis, R. Sharma and A. Brandenburg, *Backreaction of axion- $SU(2)$ dynamics during inflation*, JCAP 04 (2024) 018 [2311.07557].

[43] Z.-G. Mou, P.M. Saffin and A. Tranberg, *Simulations of Cold Electroweak Baryogenesis: hypercharge $U(1)$ and the creation of helical magnetic fields*, JHEP 06 (2017) 075 [1704.08888].

[44] S.Y. Khlebnikov and I.I. Tkachev, *Classical decay of inflaton*, Phys. Rev. Lett. 77 (1996) 219 [hep-ph/9603378].

[45] A. Rajantie, P.M. Saffin and E.J. Copeland, *Electroweak preheating on a lattice*, Phys. Rev. D 63 (2001) 123512 [hep-ph/0012097].

[46] A. Maleknejad and M.M. Sheikh-Jabbari, *Gauge-flation: Inflation from non-Abelian gauge fields*, Phys. Lett. B 723 (2013) 224 [1102.1513].

[47] P. Adshead and M. Wyman, *Natural Inflation on a Steep Potential with Classical Non-Abelian Gauge Fields*, Phys. Rev. Lett. 108 (2012) 261302 [1202.2366].

[48] D.G. Figueroa, A. Florio, F. Torrenti and W. Valkenburg, *The art of simulating the early Universe. Part I. Integration techniques and canonical cases*, JCAP 04 (2021) 035 [2006.15122].

[49] D.G. Figueroa, A. Florio, F. Torrenti and W. Valkenburg, *CosmoLattice: A modern code for lattice simulations of scalar and gauge field dynamics in an expanding universe*, Comput. Phys. Commun. 283 (2023) 108586 [2102.01031].

[50] A. Bazavov, *Commutator-free Lie group methods with minimum storage requirements and reuse of exponentials*, BIT Numerical Mathematics 62 (2022) 745 [2007.04225].

[51] A. Bazavov and T. Chuna, *Efficient integration of gradient flow in lattice gauge theory and properties of low-storage commutator-free Lie group methods*, [2101.05320].

[52] J. Ambjørn, T. Askgaard, H. Porter and M.E. Shaposhnikov, *Sphaleron transitions and baryon asymmetry: A numerical, real-time analysis*, Nucl. Phys. B 353 (1991) 346.

[53] G.D. Moore, *Motion of Chern-Simons number at high temperatures under a chemical potential*, Nucl. Phys. B 480 (1996) 657 [hep-ph/9603384].

[54] P. Di Vecchia, K. Fabricius, G.C. Rossi and G. Veneziano, *Preliminary evidence for $U_A(1)$ breaking in QCD from lattice calculations*, Nucl. Phys. B 192 (1981) 392.

- [55] I.T. Drummond, S. Duane and R.R. Horgan, *The stochastic method for numerical simulations: Higher order corrections*, Nucl. Phys. B 220 (1983) 119.
- [56] J. Berges, K. Boguslavski, S. Schlichting and R. Venugopalan, *Universal attractor in a highly occupied non-Abelian plasma*, Phys. Rev. D 89 (2014) 114007 [1311.3005].